Hot Air, Hot Lakes, or both? Exploring Mid-Holocene African Temperatures using Proxy System Modeling

Sylvia G. Dee[1], Carrie Morrill[2], Seung Hye Kim[1], James M. Russell[3]

[1]*Department of Earth, Environmental, and Planetary Sciences, Rice University, Houston, TX 77005*

[2]*Cooperative Institute for Research in Environmental Sciences, University of Colorado, Boulder, CO 80309, NOAAs National Centers for Environmental Information, Boulder, CO 80305*

[3]*Department of Earth, Environmental, and Planetary Sciences, Brown University, Providence, RI 02912*

Abstract

Climate models predict Africa will warm by up to 5°C in the coming century, stressing African societies. To provide independent constraints on model predictions, this study compares two notable reconstructions of East African temperatures to those predicted by Paleoclimate Model Intercomparison Project (PMIP3) and transient TraCE simulations, focusing on the Mid-Holocene (MH, 5-8 kyr B.P.). Reconstructions of tropical African temperature derived from lake sedimentary archives indicate 1-2.5°C of warming during the MH relative to the 20th century, but most climate models do not replicate the warming observed in these paleoclimate data. We investigate this discrepancy using a new lake proxy system model, with attention to the (potentially non-stationary) relationship between lake temperature and air temperature. We find amplified lake surface temperature changes compared to air temperature during the MH due to heightened seasonality and precessional forcing. Lacustrine processes account for some of the warming, and highlight how the lake heat budget leads to a rectification of the seasonal cycle; however, the simulated lake heating bias is insufficient to reconcile the full discrepancy between the models and the proxy-derived MH warming. We find further evidence of changes in mixing depth over time, potentially driven by changes in cloud cover and shortwave radiative fluxes penetrating the lake surface. This may confound interpretation for GDGT compounds which exist in the mixed layer, and suggests a need for independent constraints on mixed layer depth. This work provides a new interpretive framework for invaluable paleoclimate records of temperature

changes over the African continent.

Keywords: Africa, Climate Change, Lake Sediments, Paleoclimate

Key Points

- African temperature reconstructions suggest 1-2C of warming during the Mid-Holocene compared to the modern.
- Climate models cannot replicate this warming, even in combination with a lake proxy system model.
- Africa is projected to warm more than any other continent; hotter paleoclimate mean state targets must guide refinement of model physics.

1. Introduction

The African continent sustains a population of 1.2 billion people and some of the most unique and diverse ecosystems on Earth. Africa's future is made uncertain by climate model projections of severe anthropogenic warming over the next several decades and the hydroclimatic change that may accompany rising temperatures [IPCC, 2013]. As one example, regional droughts in Africa have displaced millions of people and sparked outbreaks of civil violence in multiple countries [von Uexkull, 2014, Tierney et al., 2015, Detges, 2016, Linke et al., 2018]. Given the myriad geopolitical and climatic risks that will accompany climate change impacts on Africa's developing nations, it is crucial to provide robust constraints on climate model projections of future warming in Africa.

To this end, reconstructions of climate change in Africa spanning major changes in boundary conditions (i.e. mean state changes in response to external forcing scenarios) can bolster our understanding of African climate dynamics, providing constraints on the rates and patterns of temperature and precipitation changes, as well as providing insight toward the drivers of those changes. Globally, reconstructions of the last glacial maximum [Waelbroeck et al., 2009] and others spanning the last 20kyr [Clark et al., 2012] show large changes in mean climate dominated by deglacial warming. This warming was initiated by rising summer insolation in the northern hemisphere and globally synchronized by rising greenhouse gases (GHGs) [Alley and Clark, 1999, Ruddiman, 2003, Shakun and Carlson, 2010] (Fig. 1), and was further punctuated by abrupt climate change events including Heinrich 1 and the Younger Dryas [Shakun and Carlson, 2010, Alley, 2000]. While these and other studies document global and high-latitude climate changes on centennial-millennial timescales, temperature reconstructions from the terrestrial tropics are sparse. In contrast to the robust body of work constraining hydroclimate changes in Africa [e.g. Tierney et al., 2008, 2011, Russell et al., 2014, Tierney et al., 2015, and many others], reconstructions of African temperature spanning large climate transitions are sparse, and much of Africa's *thermal* past remains opaque.

During the last decade, the application of organic geochemical temperature proxies based upon glycerol dialkyl glycerol tetraethers (GDGTs) in lake sediment cores has begun to fill in the gaps in reconstructions of African temperature change [Powers et al., 2010, Tierney et al., 2010c]. In particular, recent work has demonstrated that multiple paleoclimate proxy records (GDGTs and others) show evidence for warmer temperatures during the Mid-Holocene (MH hereafter), ∼6 ka [Powers et al., 2005, Tierney et al., 2008, Berke et al., 2012b]. Reconstructions from multiple sites in Africa indicate warming of 1-3°C [Tierney et al., 2008, Powers et al., 2005] relative to the pre-industrial (PI) period. Remarkably, this reconstructed period of African warming occurred when insolation and greenhouse gas forcing were near their Holocene minima (Figure 1) [Joos and Spahni, 2008]. Thus, various hypotheses have been proposed to explain these observations, from teleconnections between tropical Africa and the high latitudes, to biases in the temperature proxies introduced by lake processes such as mixing. Indeed, this large, sustained warming event (the largest after the glacial termination on the African continent) occurred near the end of the African Humid Period, potentially invoking feedbacks between temperature and the hydrological cycle [Gasse, 2000]. To date, however, little attempt has been made to examine the energy transfers required to produce the observed high temperatures during the MH.

What are the drivers and processes that could explain prolonged temperature change on a tropical land mass? Via joint evaluation of climate model simulations and proxy system biases, this work seeks to deconvolve the relationships between reconstructed lake surface and GCM-simulated air temperature during the 6 ka thermal maximum inferred from lake records. The GDGT proxy records lake temperature rather than the primary variable of interest (simulated by climate models): air temperature. The relationship between lake and air temperatures is potentially nonstationary, and depends on lake heat budget and mixing regimes [Dee et al., 2018]. To diagnose the dynamics and sensitivity of tropical African temperature changes during the MH warming event, this work pursues a novel, integrated data-model comparison study to evaluate air and lake temperatures over the last

10 kyr. Focusing on geochemical reconstructions of temperature from equatorial African lakes Malawi and Tanganyika [Tierney et al., 2008, Powers et al., 2005], reconstructions are compared to coupled general circulation model (GCM) simulations spanning 100 years of the mid-Holocene (MH), pre-industrial (PI) and the historical period (HIST). Note that MH and PI experiments are driven with an annual cycle of external forcing with boundary conditions consistent with the target time period, and do not span 'real' time in years (similar to a control simulation). Full analysis of the multi-model spread is used to probe the mechanisms that control the rate and amplitude of simulated temperature changes in the MH. To quantify uncertainties related to the lake system impacts on proxy reconstructions (e.g. lake energy balance and temperature profile, mixing, sedimentation, and bioturbation), we apply a new Proxy System Model (PSM) for lakes to translate climate model output to lake surface temperature and mixing depth reconstructions and better quantify proxy system uncertainties [Dee et al., 2018]. Comparison of geochemical proxy records with PSM output and transient and time-slice paleoclimate simulations from GCMs reveals large discrepancies between simulated and reconstructed temperatures; the potential causes of these discrepancies are evaluated in succession.

2. Methods

2.1. GDGT Temperature Reconstructions from African Lakes

The development and application of glycerol dialkyl glycerol tetraether (GDGTs) temperature proxies have provided invaluable time-continuous records of tropical continental temperature changes. GDGTs are membrane-spanning lipids that include isoprenoidal GDGTs (iGDGTs), produced by Thaumarchaeota and which comprise the TetraEther indeX of tetraethers with 86 carbon atoms (TEX_{86}), and branched GDGTs (brGDGTs) thought to be produced by Acidobacteria that form the basis for the Methylation of Branched Tetraether (MBT) and the Cyclisation of Branched Tetraether (CBT) MBT-CBT proxy [Schouten et al., 2002, Weijers et al., 2007]. The proxies are based on the fact that microbes vary the number of ring structures and/or methyl branches in GDGT alkyl chains in response to environmental conditions, including temperature [Schouten et al., 2012, Russell et al., 2018]. The use of TEX_{86} as a temperature proxy is restricted to large lakes because iGDGTs in small lakes tend to be contaminated with compounds from surrounding shoreline soils [Castañeda and Schouten, 2011, Powers et al., 2010].

Site	Lat/Long	Elevation (m a.s.l.)	Time-span (ka)	Resolution (yr/sample)	Calibration Uncertainty	Analytical Uncertainty	Data Source
L. Malawi	12.5°S, 36°E	500	25 - present	600	3.6°C	< 1°C	[Powers et al., 2005, 2010]
L. Tanganyika	6.5°S, 30°E	773	60 - present	250	3.7°C	0.3°C	[Tierney et al., 2008]

Table 1: Details of the GDGT temperature reconstructions from tropical Africa examined in this work: site, location, time span, temporal resolution, calibration uncertainty (from original publications), and analytical uncertainty. Note that calibration + analytical uncertainties applied to analysis in this paper is based on updated calibration uncertainty estimation presented in Tierney et al. [2010a].

GDGTs have been applied to multiple sites in Africa and have produced reproducible temperature histories (Fig. 2), including reconstructions that span the MH. The two records we draw from in this paper are detailed in Table 1, and reconstructed temperature anomalies across the Holocene are shown in Fig. 2b. We focus on these records in particular because both sites have well documented limnological data, and the Tanganyika record in particular is considered 'emblematic' of climate changes in equatorial Africa [Tierney et al., 2008, Powers et al., 2005]. In general, reconstructions from these two sites have yielded some of the most complete, time-continuous temperature records from the continental tropics, and have provided many fundamentally important inferences [Berke et al., 2012b,a, Castañeda and Schouten, 2011, Weijers et al., 2007, Loomis et al., 2012, 2017, Morrissey et al., 2017, Powers et al., 2005, Tierney et al., 2008].

Lake Malawi records a Holocene thermal maximum at 5 ka, followed by $\sim 1.5°C$ cooling to the PI (Fig. 2b). Despite substantial differences between the two records during the earlier Holocene, a 60-ka record from Lake Tanganyika, SE Africa replicates many features of Lake Malawi, including the MH thermal maximum at 5 ka (Tierney et al., 2008). Both lakes indicate the MH was $\sim$1.5-2.5$°C$ warmer than the PI and thus likely $\sim$1-2$°C$ warmer than the historical period, considering anthropogenic warming). However, the reconstructed warming exhibits differences in timing and amplitude between the two records (e.g. Fig. 2b., see evolution of reconstructions across the 6 ka time horizon). This could indicate that either: 1) the climate signal is regionally heterogeneous, or 2) the lake system influences the amplitude and trajectory of the recorded warming. For 2), the lake proxy system model is able to partition the lake heat budget contribution to the overall reconstructed temperature signal, and evaluate seasonal biases. These tests are discussed in Section 3. Lake reconstruction sites are evaluated relative to climate model simulations to diagnose large-scale temperature changes in Africa.

2.2. Climate Model Experiments

To diagnose the drivers of temperature signals across the MH inferred from lake sedimentary archives, we employ climate model simulations from the Paleoclimate Modelling Intercomparison Project (PMIP3) [Braconnot et al., 2012, Meinshausen et al., 2011]. We employ PMIP3 models that ran MH, PI, and HIST simulations ($n = 13$, details in Table 2) in this work to examine African temperatures during the MH period compared to the historical period and the PI. PMIP3 MH and PI simulations are equilibrium simulations with uniform forcing from which we obtained 100 years of output; the historical simulations are transient runs spanning the period 1850 to 2005. We calculated both [MH - PIcontrol] and [MH-HIST] anomalies for each simulation in the ensemble (Sec. 3). Multi-model HIST-PI air temperature differences are approximately 0.3°C and 0.2°C for Tanganyika and Malawi, respectively. We additionally applied a calendar-correction to the MH simulations per the methodology described in Bartlein and Shafer [2019] to account for changes in month length and seasonality over time forced by changes in eccentricity and precession (SI Fig. S2, S3). The multi-model ensemble of PMIP time slice experiments is used to identify differences in radiation and heat transport, surface energy balance forcings and feedbacks. Climate fields were extracted for the grid cells which cover Lakes Tanganyika and Malawi, and post-processed to drive the lake proxy system model (Sec. 2.3). (Note that we used all grid cells intersecting with lake area rather than a single grid cell corresponding to core sites. However, comparing the grid cells used to the maps from each model, grid cells with negligible lake area were not included; only grid cells that collectively covered the majority of the lake area are selected).

Second, we used the TraCE-21ka (Transient Climate Evolution of the last 21,000 years) simulation for an additional comparison of a simulated surface air temperature time series with temperature reconstructions from Tanganyika and Malawi (see Fig. 2). The TraCE-21ka simulation was completed with the fully-coupled Community Climate System Model, version 3 (CCSM3), run without time acceleration at the T31_gx3 resolution [Liu et al., 2009, He, 2011]. The prescribed, time-varying forcings for this simulation are orbitally-forced insolation and atmospheric greenhouse gas concentrations. Specified boundary conditions include ice sheet extent and height from the ICE-5G reconstruction, coastline changes resulting from rising sea levels, and freshwater forcing from retreating ice sheets to the North Atlantic and Southern Oceans [Liu et al., 2009, He, 2011].

Model name	Atm. resolution lat x lon (levels)	Ocn. resolution lat x lon (levels)	Model years (MH)	HIST ensemble members	Tanganyika Grid Cells	Malawi Grid Cells	Reference
BCC CSM1.1	64 x 128 (26)	232 x 360 (30)	1-100	3	2	2	Wu et al. (2013)
CCSM4	192 x 288 (26)	384 x 320 (40)	1000-1099	3	4	5	Gent et al. (2011)
CNRM-CM5	128 x 256 (31)	292 x 362 (42)	1950-2049	3	4	3	Voldoire et al. (2013)
CSIRO Mk3.6.0	96 x 192 (18)	189 x 192 (31)	1-100	3	3	3	Rotstayn et al. (2010)
FGOALS-g2	60 x 128 (26)	196 x 360 (30)	920-1019	3	2	2	Li et al. (2013)
FGOALS-s2	108 x 128 (26)	196 x 360 (30)	1-100	2	3	4	Bao et al. (2013)
GISS-E2-R	90 x 144 (40)	180 x 288 (32)	2500-2599	3	3	2	Schmidt et al. (2014)
HadGEM2-ES	145 x 192 (38)	216 x 360 (40)	2061-2160	3	4	4	Johns et al. (2006)
IPSL-CM5A-LR	95 x 96 (39)	149 x 182 (31)	2301-2400	3	3	3	Kageyama et al. (2013)
MIROC-ESM	64 x 128 (80)	192 x 256 (44)	2330-2429	3	2	2	Watanabe et al. (2011)
MPI-ESM-P p1	96 x 192 (47)	220 x 256 (40)	1850-1949	2	3	3	Giorgetta et al. (2013)
MPI-ESM-P p2	96 x 192 (47)	220 x 256 (40)	1850-1949	2	3	3	Giorgetta et al. (2013)
MRI-CGCM3	160 x 320 (48)	368 x 364 (51)	1951-2050	3	5	4	Yukimoto et al. (2012)

Table 2: PMIP3 simulation details for models used in this study. Columns from left to right: model name, atmospheric resolution (lat, lon, levels), ocean resolution (lat, lon, levels), model simulation years for the Mid-Holocene run, number of HIST ensemble members, number of model grid cells spanning Lake Tanganyika, number of model grid cells spanning Lake Malawi, and reference. The 'model years' do not refer to calendar years C.E. or B.P.; rather, these are simply arbitrary run years chosen for the PMIP3 submission, and are provided here for reproducibility.

2.3. Lake Proxy System Model

Proxy system models (PSMs) are now widely used tools for translating climate model variables (e.g. temperature or precipitation) to a paleoclimate archive signal (e.g. oxygen isotopes in ice cores), placing model data in the same units or reference frame as the measured proxy data [and see Evans et al., 2013, Dee et al., 2015, 2018, for a review]. PSM simulations translate GCM output into quantities directly comparable to proxy measurements, more completely quantifying proxy uncertainty. The lake proxy system model (PSM) bridges climate model output with the proxy data by modeling the lake system itself. Here, we use a recently developed full lake PSM from the PRYSM framework [Dee et al., 2018]. The PSM is fully described in Dee et al. [2018]; briefly, the PSM simulates physical processes that impact the lake energy and water balance and thus temperature, but also integrates and compounds multiple sources of uncertainty related to how proxy signals settle in sediments (e.g., bioturbation), dating, and proxy calibration.

The proxy system model requires several inputs including air temperature, humidity, wind speed, downward long/shortwave radiation, and surface pressure; a schematic of the heat budget of the Lake PSM is given in Figure 3. To simulate changes between the MH and HIST periods, we first calibrated several lake-specific parameters in the lake model by driving the model for both Tanganyika and Malawi with reanalysis data spanning 1979-2005 (ERA-Interim Reanalysis) [Dee et al., 2011] and comparing simulated lake temperature, evaporation, and mixing depth to modern observations.

Model parameters calibrated include the neutral drag coefficient (C_D) and the shortwave radiation penetration depth parameter (η) [and see Dee et al., 2018, for more detail]. The historical period in this paper is thus defined as the years spanned by the reanalysis product. The annual cycle was then computed using the PSM output to produce an average historical year. To simulate changes in the MH, the 12-month annual cycle for the PMIP3-defined HIST and MH time slice data were extracted for all 13 models. For the MH simulations, we averaged 100 years of model output, and for the CMIP HIST experiments, we averaged across multiple realizations for each model in order to improve the statistical representation of the relatively short 1979-2005 time period (specifics of the PMIP3 simulations are detailed in Tab. 2). We scaled the lake model input fields by computing either the direct MH-HIST anomalies (temperature), or the percent change in the MH compared to HIST time slices, $[(MH - HIST)/HIST \cdot 100]$ (all other input fields). We then applied those anomalies or percent changes to the average seasonal cycle in ERA-Interim (sometimes referred to as a δ method). Specifically, we computed the annual climatology of the reanalysis data, taking the average for each individual calendar month, and applied the [MH-HIST] δ's of each model-simulated month to the modern climatology. This procedure generates one MH input file for the LakePSM from each of the 13 PMIP3 model simulations. Each of the resulting 13 MH LakePSM simulations share the same modern control simulation (i.e., the LakePSM forced with ERA-Interim inputs). (Note that this process is designed to maintain consistency in the calibrated model averages during the historical period; the requirement of calibration of the lake model simulation using observations motivates comparison of MH vs. HIST as opposed to MH vs. PI). Scaling modern reanalysis data to the simulated [Paleo-Modern] anomalies circumnavigates the climatological biases in the PMIP3 models [e.g. Lorenz et al., 2016].

2.4. Model Performance

The lake proxy system model simulates variables including water temperatures, lake mixing depth, and evaporation rate. We first assessed the performance of the model forced with ERA-Interim fields for both lakes [and see Dee et al., 2018]. Modeled and observed (*in-situ* [G Kumambala and Ervine, 2010, Eccles, 1974, Kumar et al., 2019] and satellite-derived [Kraemer et al., 2015, Wooster et al., 2001]) lake surface temperatures, evaporation rates, and mixing depths over the historical period are compared in Table 3. Note that for both lakes, the general climatology consists of a wet season during austral summer ($\sim$ONDJFM) and a dry season during austral

Climate/Lake Variable	Observed Wet Season (ONDJFM)	Modeled Wet Season	Observed Dry Season (AMJJAS)	Modeled Dry Season
Tanganyika				
In Situ Surface Temperature (°C)	27.8 ± 0.7°C	28.7°C	23 ± 0.9 °C	23.0°C
Satellite-Derived Surface Temperature (°C)	28.5°C	28.7°C	23.5°C	23.0°C
Evaporation (mm/day)	3 mm/day	4 mm/day	6 mm/day	4 mm/day
Mixing Depth (m)	50 ± 10m	30m	90± 10m	85m
Malawi				
In Situ Surface Temperature (°C)	28°C	30°C	22.6°C	22°C
Satellite-Derived Surface Temperature (°C)	28°C	30°C	23°C	22°C
Evaporation (mm/day)	(see caption)	2 mm/day	(see caption)	5 mm/day
Mixing Depth (m)	50 m	14m	200m	41m

Table 3: Comparison between observations from Lake Tanganyika vs. Lake PSM-simulated conditions, forcing the lake model with ERA-Interim reanalysis data for the region. Available observations spanning the last few decades for Lake Tanganyika include surface temperature, evaporation, and mixing depths [Eccles, 1974, Kumar et al., 2019, Kraemer et al., 2015]. Previous work documents *in-situ* annual average evaporation rates at Malawi of approximately 4.5-5.2 mm/day [G Kumambala and Ervine, 2010, Eccles, 1974]. Seasonal temperature variability is documented for Malawi in [Wooster et al., 2001]. Note that wet season months span (ONDJFM); dry season months (AMJJAS).

winter (∼AMJJAS). The PSM simulates seasonal variations in lake surface temperatures in general agreement with modern observations, though the simulated seasonal cycles in both evaporation and mixing depth in the wet season are underestimated (and this bias is larger for relatively shallow simulated mixing depths in Lake Malawi). The large mixing depth bias for Lake Malawi is potentially driven in part by the fact that the LakePSM used in this paper [Dee et al., 2018] is a one-dimensional model, and does not simulate lake dynamics such as wind-driven, north-south oscillations in thermocline depth in narrow lakes such as Malawi and Tanganyika, a key control on observed mixing depths [Naithani et al., 2003, Eccles, 1974]. In particular, observations of mixing depth and lake surface temperature for Malawi given in Table 3 were taken at the north side of the the lake; the 1D model does not capture lake seiches that may be more prevalent at the north end of Malawi than in central Lake Tanganyika. Finally, it is also possible that ERA-Interim input values are biased for Malawi, where fewer meteorological station observations are available, limiting our ability to accurately tune model parameters over the historical period.

3. Results

The warming temperatures across 6ka reconstructed from GDGTs in Lake Tanganyika and Lake Malawi could result from a variety of processes, including regional feedbacks that influence the local radiation balance, or changes in heat export from the tropics related to high latitude warming or cooling. We disentangle the impacts of both climate and proxy system (lake system) processes in the analyses that follow.

3.1. Data-Model Comparison

To assess the agreement between proxy reconstructions and available GCM simulations, **[Fig. 2]** shows the mean temperature reconstruction for Lakes Tanganyika and Malawi superposed on two transient simulations spanning the Holocene: the Community Climate System Model (CCSM3) Simulation of the Transient Climate of the Last 21,000 Years (TraCE-21ka) [Liu et al., 2009], as well as the PMIP3 time slice estimates of annual-mean temperature anomalies (boxplots). Temperature anomalies for all data presented in **[Fig. 2]** were computed relative to the PI mean. Note the choice to compute anomalies relative to the PI is due to the fact that lake reconstructions (GDGT records) do not extend into the historical period. The reconstructions are coarse temporally compared to the model simulations. The two PI time periods for the reconstructions were taken (based on the most recent measurement points) as the average of 1750 B.P. (200 C.E.) to 250 B.P. (1700 C.E.) for Malawi (n = 3) and 2818 B.P. (-868 CE) to 1313 B.P. (637 C.E.) for Tanganyika (n = 6). Given the differences in dating resolution in the two reconstructions as well as their top-most dates (given above), these two time periods were taken as reasonable choices to represent PI climate. Similarly, for the Mid-Holocene averages, we restricted the calculation to times falling in the interval 4500:6800 B.P. (Tanganyika n = 10 data points, Malawi n = 5 data points). The MH average temperatures are extracted from each record over a 2000-year interval of core spanning multiple ^{14}C ages within each section. Dating uncertainties for both sites are on the order of ±200 years [Tierney et al., 2008, Johnson et al., 2002]. Each interval is bracketed by several dates with uncertainties much smaller than the averaging period length, making it unlikely that age uncertainties affect the analysis presented here.

The lake reconstructions and model simulations notably diverge due to the lack of simulated MH warming in model experiments compared to the GDGT reconstructions. The models do not capture the magnitude nor the trend of MH warming observed in Lakes Tanganyika and Malawi across this boundary, though this assertion is contingent upon calibration uncertainties in the GDGT reconstructions (Table 1). Quantifying this difference, Table 4 lists [MH minus HIST] annual average air temperature anomalies for model grid cells centered over both lakes in the PMIP3 ensemble alongside GDGT-derived estimates, including uncertainties; [MH-PI] values for the proxy records are also given for reference. Of the 13 PMIP3 simulations we analyzed, 12 simulate colder MH temperatures compared to the historical simulations at both lake sites; all 13 indicate a colder MH compared to PI. This contrasts with the lake temperature reconstructions (Fig. 2b), which indicate MH temperatures in equatorial Africa 1-2.5° warmer than the pre-industrial (Tab. 4). The one notable exception is HadGEM-2; the average air temperatures over Tanganyika are equal to those of the historical time slices in the MH, and hotter over Lake Malawi. HadGEM-2 is thus the only PMIP3 model showing MH temperatures similar to or warmer than the historical period.

It is important to explicitly consider uncertainties for all data types in the comparison. Uncertainty bounds for the proxy estimates of MH-HIST temperature changes were derived using bootstrapped re-sampling of the calibration uncertainty (resulting in a value of $\sigma = \pm 0.4°C$) as computed in Tierney et al. [2010a]. PMIP3 model uncertainties are computed by calculating the standard deviation of the [MH-PI] and [MH-HIST] differences for the model ensemble (in terms of mean annual air temperature), and are approximately equal to $\pm 0.3°C$ (Table 4). Finally, the LakePSM uncertainty was calculated using a perturbed-parameter ensemble (Sec. S2) and repeating the same method used for the PMIP3 simulations, calculating the standard deviation of the [MH-PI] and [MH-HIST] differences for the model ensemble of mean annual lake surface temperatures. The PSM uncertainties associated with selection of parameter value are small, $\sim \pm 0.04°C$.

3.2. Impact of Lake System Biases

While the lack of data-model agreement could be attributed to shortcomings in climate model physics, it is also necessarily to evaluate biases imparted by the lake system. While GDGT proxies are potentially an unbiased indicator of lake temperature, issues may arise when lake temperature is assumed equal to air temperature. In particular, changes in lake water column surface energy fluxes or mixing can alter the air-lake temperature relationship: lake temperatures may be damped or amplified compared to air temperature changes due to mixing (e.g. changes in thermocline depth) and the high specific heat capacity of water [Dee et al., 2018]. Furthermore, Supplementary Table S0 indicates that while most of the African Great Lakes measured surface temperatures are systematically higher than reanalysis air temperatures, there is large regional heterogeneity in the lake-air temperature offset in the modern [Green, 2009, Turner et al., 1996, Minale, 2020, Spigel and Coulter, 2019]. Air-lake temperature relationships may also be non-stationary. Taken together, these uncertainties beg the question: how much (if at all) are lake temperature reconstructions biased relative to air temperature?

Reconstructed lake temperatures at ∼6 ka coincide with enhanced fall insolation during the MH. In the model simulations, the enhanced JJASON

PMIP3 MODEL	**[MH-HIST] MAAT ($^{\circ}C$) (Tanganyika)**	**[MH-HIST] MAAT ($^{\circ}C$) (Malawi)**
BCC	-0.70	-0.45
CCSM	-0.51	-0.37
CNRM	-0.64	-0.49
CSIRO	-0.44	-0.39
FGOALS-g2	-0.80	-0.71
FGOALS-s2	-0.91	-0.63
GISS	-1.28	-0.51
HADGEM-2	**0.0**	**+0.37**
IPSL	-0.76	-0.59
MIROC	-0.34	-0.21
MPIp1	-0.70	-0.42
MPIp2	-0.79	-0.37
MRI	-0.51	-0.29
PMIP3 [MH-HIST] MEAN	-0.7 ± 0.31	-0.4 ±0.27
PMIP3 [MH-PI] MEAN	-0.3 ±0.34	-0.2 ±0.13
GDGT MH-PI	+1.4 ±0.4	+1.9 ±0.4

Table 4: **PMIP3 Mid Holocene Air Temperature Anomalies.** PMIP3 MidHolocene minus Historical Mean Annual Air Temperature at Lakes Tanganyika & Malawi. Top 14 rows show the change in PMIP3 model estimates for the difference in MH and HIST air temperatures and the PMIP3 multi-model mean; bottom row indicates the estimated warming during the MH compared to the pre-industrial (PI) and observed historical period from GDGT reconstructions of both lakes. The GDGT reconstruction anomalies are reported for MH relative to PI; the proxy data does not extend through the modern period. Note GDGT difference is given with calibration uncertainty ($\sigma = \pm 0.4^{\circ}C$) as computed in Tierney et al. [2010a]; the PMIP3 model uncertainties are computed by calculating the standard deviation of the [MH-PI] and [MH-HIST] differences for the model ensemble (in terms of mean annual air temperature). For reference, the PMIP3 HIST-PI multi-model air temperature mean is approximately 0.3°C for Tanganyika, and 0.2°C for Malawi.

insolation results in elevated SON temperatures throughout the MH. This result is consistent for PSM simulations using both the calendar-corrected and un-corrected input data, indicating the correction is negligible in the context of this analysis (Figs. S2, S3). Figure 4 shows seasonal temperature anomalies across the African continent (MH minus historical), using the warmest MH PMIP3 simulation (HadGEM2). The stronger seasonality of air temperature during MH is apparent, with much colder temperatures over much of Africa during DJF and MAM, and warmer temperatures (by up to 3°C) during JJA and SON, especially in the great lakes regions.

These lakes gain most of their annual heat budget during austral spring (SON) after winter mixing (when lake heat budgets are sensitive to temperature fluxes), and thus several studies have invoked the increase in SON insolation to explain the elevated MH lake warming signal, focusing on processes such as mixing internal to the lake [Tierney et al., 2010b, Berke et al., 2012b, and see Section 3.3]. Testing this directly, Figure 5 shows the seasonal cycle of both air temperatures and lake surface temperatures (generated using the lake PSM forced with HadGEM2 inputs) for both the MH and historical periods at Lake Tanganyika. The calendar-corrected MH data are also reproduced in all four panels of Fig. 5 (red curve). Comparison with ERA-interim reanalysis air temperatures (dashed line, superimposed on Fig. 5) indicates that despite bias in HadGEM2 air temperatures, which are higher than observations during winter months (November-March), the model does accurately simulate the observed seasonal cycle for lake surface temperature (Table 2).

Annual average temperature changes for HadGEM2 are summarized in Table 5. The annual average HadGEM2 air temperatures simulated during both the historical and mid Holocene time slices are equivalent, $\sim$ 22°C. However, as shown in Fig. 5a., there is enhanced seasonality over equatorial Africa due to precessional forcing during the MH, and the region received more solar radiation in JJA/SON. Conversely, Fig. 5b. shows that lake surface temperatures **[are generally higher throughout ASOND in the MH]**, *despite no change in annual average air temperatures between MH and HIST*. This implies a non-stationary temperature bias between air and lake temperature (the air-lake temperature offset changes in different climate states), arising due to lake heat budget effects alone.

We repeated this analysis for the full PMIP3 ensemble and for both lakes, generating MH input files for the LakePSM from each PMIP3 model using the approach described in Section 2.3. MH vs. HIST air temperature anomalies were compared to lake temperature anomalies (expanding Table 5 for the full PMIP3 ensemble). The total lake amplification of air temper-

Time Slice	**Air / Lake Temperatures**
$HIST_{AIR}$	21.9°C
MH_{AIR}	21.9°C
Air Anomaly	0
$HIST_{LAKE}$	26.5 °C
MH_{LAKE}	27.3 °C
Lake Anomaly	0.8
Bias (Lake-Air)	**0.8**

Table 5: HADGEM-2 MidHolocene (MH) vs. Historical (HIST) Mean Annual Air Temperature and Lake Surface Temperature simulated at Lake Tanganyika. Lake PSM uncertainties are approximately $\pm 0.04C$ (Sec. S2).

atures (MH minus HIST) is shown in Figure 6. This yields a multi-model average of 0.3°C hotter and 0.05°C colder lake surface temperatures than air temperatures for MH compared to HIST at Tanganyika and Malawi, respectively. This temperature bias is larger for Tanganyika (see Sec. 3.3).

BCC is a notable outlier in Figure 6, and shows a large cold bias for both lakes. While its air temperature anomalies are comparable to other models (Tab. 4), BCC's wind speed anomalies greatly exceed other models during the MH (a 124% increase), amplifying lake cooling (not shown). However, the model only drives down the multi-model average by approximately 0.1°C, for reference.

To test the hypothesis that MH insolation forcing imparts a seasonal bias on the lake surface temperature reconstructions and to diagnose the energy balance changes involved, we examined the changes in the lake energy budget terms in HADGEM-2 (Fig. 3): lake surface temperature, downwelling shortwave, downwelling longwave, upwelling shortwave, upwelling longwave, sensible heat flux, and latent heat flux (Figs. 7,8).

The simulation's seasonal cycle indicates more longwave radiation and less net shortwave radiation (SW hereafter) at the lake surface (Figs. 7, 8, S6) and higher humidity during the wet season (∼ONDJFM). By contrast, the dry season (∼AMJJAS) is drier, sunnier, and windier. The timing of the wet season and the dry season is similar between Tanganyika and Malawi. The warmest lake temperatures happen at the end of the wet season and the coolest lake temperatures happen at the end of the dry season. Latent heat fluxes likely play an important role in this cycle. There is much more evaporation during the dry season than during the wet (a seasonal range of 175 W/m^2 at Tanganyika). So, despite increased SW radiation during the dry season, increased evaporative cooling of the lake (drier, windier conditions) and decreased downwelling longwave (likely due to reduced cloud cover, see Sec. 3.3) would act to cool both Tanganyika and Malawi.

Figures 7 & 8 indicate coherent changes during the MH in the surface heat budgets: alongside higher lake surface temperatures during ASOND, we observe elevated downwelling SW radiation, small-negligible changes in sensible heating, and enhanced upwelling longwave radiation. These changes are robust to changes simulated using calendar-corrected MH forcing (SI, Figs. S2, S3). Interestingly, latent heat is less negative during AMJJASO in the MH simulation compared to HIST, indicating reduced heat loss and reduced evaporative cooling (Figs. 7c., 8c., S6) during this season. By contrast, for Lake Malawi (Fig. 8), evaporation and latent heat release increase during SON, suggesting the enhanced evaporation and latent heat release cannot explain the enhanced warming at 6ka. Rather, the variable which shows consistently higher (though modest $\sim 20W/m^2$) values during JJASON (austral winter, spring, i.e. the lakes' dry season) is downwelling SW radiation. The seasonality impact on lake temperature is asymmetric: the enhanced wet season warming is not fully offset by dry season cooling due to enhanced temperature seasonality and cloud cover change.

Furthermore, in the MH compared to PI, transitions between wet/dry seasons are shifted such that seasonal changes occur earlier in the year. Due to orbital forcing, incident SW radiation is elevated during JJA and SON in the MH for all 13 PMIP3 models (SI, Fig. S1). Cloud feedbacks could potentially accentuate changes in August and September (the months with greatest orbital forcing at 6 ka) insolation through October and November.

In the simulation, lake surface temperatures do not directly track changes in annual average air temperatures. Because GCMs simulate air temperatures only, it follows that a direct comparison between lake surface temperature reconstructions and air temperature simulations from GCMs may contain uncertainties generated by lake system dynamics. The above analysis suggests a substantial amount of the warming recorded by lake GDGT archives may arise from the lake energy budget alone. The PMIP3 multi-model range indicates lake heat amplification due to enhanced MH JJA/SON heating may account for between 0 to 1.5 °C of reconstructed warming observed in GDGT-based reconstructions, despite little-no change in annual average air temperatures. However, lake heat budget biases cannot reconcile *all* of the proxy-reconstructed warming during the MH. The multi-model average lake temperature bias compared to air temperatures is 0.3°C, and only partially accounts for the data-model MH gap.

Revisiting our motivating question, *how does the lake system itself alter the signal?*, the apparent lake heating bias shown in Fig. 5 and the analysis discussed above suggests MH insolation forcing drives seasonal biases causing enhanced JJA-SON heat uptake, contributing to observed MH warming in Tanganyika and Malawi. This observation warrants further investigation, however: *What are the explicit physical impacts of enhanced solar radiation seasonality on the lake energy budget, and why does this elevate lake surface temperature?* Furthermore, other lake-specific processes can affect the reconstructed temperature signal, such as mixing depth. These additional mechanisms for heightened sensitivity to enhanced MH JJA-SON insolation are discussed in Section 3.3.

3.3. Coupled Climate-Lake Dynamics: Mixing Depths and MH Warming

We next characterize the impacts of enhanced seasonality in SW on lake heating in the MH. Relevant are the spatial changes over Africa in surface downwelling SW radiation (Fig. 9), cloud cover, and precipitation (Fig. 10). Figure 10 shows the seasonal average anomalies in cloud area fraction (MH minus HIST). Over the great lakes region, cloud cover is reduced in MH JJA and SON relative to HIST. Lower cloud albedo leads to decreased reflection of incoming solar radiation; indeed, Figure 9 shows increased surface downwelling SW radiation corresponding to areas of lower cloud cover during the MH over Malawi and Tanganyika (JJA-SON). Increased SW radiation in JJA and SON during the MH is consistent with increased insolation driving a larger seasonal northward shift of the Tropical Rain Belt, which causes increased cloud cover north of the equator during the African Humid Period (AHP, Fig. 10, MAM, JJA), and decreased cloud cover in the south at 6 ka [Shanahan et al., 2015, Chevalier et al., 2017]. Precipitation changes are small over both lake regions during JJA/SON (Fig. 10), though the HadGEM2 model does simulate wetter ($\sim +1$ mm/day) conditions over Tanganyika during the dry season ($\sim$AMJJAS); this increase occurs despite the northward shift of the Tropical Rain Belt documented in previous work [Gasse, 2000, Shanahan et al., 2015, Costa et al., 2014]. Essentially, the model simulation suggests changes in cloud cover can promote lake warming through increasing SW radiation incident at the lake surface contemporaneously with a wetter dry season and wetter conditions in general, in agreement with previous hydroclimate reconstructions from Tanganyika [e.g. Tierney et al., 2008, Ivory and Russell, 2016]. By contrast, we note that at Malawi, previous works suggests conditions were substantially drier during the AHP [Finney and Johnson, 1991]. While the two lakes do not share the same hydrologic history, similar changes in seasonal lake temperatures and mixed layer depth underscores the importance of shortwave forcing and cloud cover, which may overcome latent heat loss and other processes likely to differ at the two lakes.

Shortwave radiation directly impacts lake surface temperature, but also exerts a primary control on mixing depth [Hostetler and Bartlein, 1990]. While mixing depth depends on multiple additional controls including surface temperature, evaporation, wind speed, and humidity, net downward SW radiation is the only variable notably enhanced in the MH. Due to the exponential decline of SW permeation with depth in the lake, an increase in surface incident shortwave radiation will heat surface waters more than deep waters, causing surface waters to become more buoyant than deeper layers and reducing mixing [see Dee et al., 2018, SI]. Figure 5c. shows the HadGEM2 MH and HIST simulations of SW radiation over Lake Tanganyika. As discussed above, and shown in Figure 5c., more SW radiation penetrates the lake surface in MAM-JJA in the MH relative to HIST; as a result, Figure 5d. shows that in HadGEM2, lake mixing depths are approximately 10-20 m shallower during MH JJA compared to historical.

The mixing climatology for both lakes are such that mixed layer depths are shallow ($\sim$20 meters) during the wet season, and deepen through the dry season with maximum mixing in September. The mixed layer deepens through the dry season due to both windier conditions and due to surface heat loss through evaporation. Deepening of the mixed layer during the dry season further contributes to lake surface temperature cooling by transferring heat to deeper layers. Figure 5b. indicates that deeper dry season mixing ends earlier (by about one month) in the MH (and see Figs. 7,8b.). This shift in the seasonal timing of lake surface temperature and mixing depth is most pronounced at the end of the dry season, which starts one month earlier during MH and leads to warm lake temperature anomalies during SOND.

This change in mixing depth seasonality occurs in both lakes, and is potentially important for understanding the biases between lake and air temperatures. Namely, reduced mixing depth results in a reduction in the ability of the lake to store heat (thus warming the surface layer). Large [MH-HIST] lake surface temperature anomalies onset in September and are maintained through November. Surface heating due to the large positive anomaly in SW radiation alone may cause the mixed layer depth to shallow. In any case, a shallowing mixed layer would act to perpetuate and enhance an initial surface heating.

In sum, during both the MH and HIST periods, mean annual temperature in the lake is set by the change in seasonal cloud cover and insolation (SW radiation). Reduced JJA-SON cloud cover and increased shortwave radiation at lake surface also directly impact mixing depth. PMIP3 simulations indicate shallower mixed layer depths during the MH relative to HIST in September-October, driven in part by greater surface incident shortwave radiation. These changes in lake stratification and mixing compound the dry season warming observed during JJA-SON, maintaining elevated MH temperatures initiated by enhanced shortwave radiation in MAM-JJA throughout SON. The dry-wet season shift from deeper to shallower mixed layers occurs one month earlier in the MH, due to increased downward SW. Increased SW forcing heats and increases the buoyancy of surface waters, and would enhance direct SW effects on lake surface temperature via shallowing the thermocline and reducing the redistribution of heat to deeper layers.

4. Discussion: Unravelling Drivers of African Temperature Changes in the Holocene

This study evaluates temperature changes in paleoclimate reconstructions and GCMs, specifically the accuracy of GCM hindcasts of past African temperature. The suite of PMIP3 models which performed a MH time-slice simulation were analyzed, and we evaluated model simulations which come closest to simulating regional reconstructed temperatures for Africa during the MH (HadGEM2). Output from the climate model simulations were then used to drive a lake PSM that simulates lake energy balance to identify processes that explain the timing and amplitude of observed African temperature signals. The PSM directly simulates lake temperature, and provides direct insights into the energy and mass transfers that drive those lake temperature changes.

The lake PSM indicates that lake and air temperatures differ in their relative means, seasonality, and patterns of change through time, indicating biases imparted by the lake system [Dee et al., 2018]. Amongst all PMIP3 models, none simulate higher mean annual air temperatures in tropical Africa during MH compared to present-day (Section 3.1). However, multiple processes within the lake proxy system alter the input air temperature signal. Employing the Lake PSM energy balance model, we converted modeled air temperature and other environmental inputs to lake surface temperatures, and in doing so quantified biases between modeled air and lake surface temperatures during the relatively warm MH. Lake temperatures are warmer during SON at 6 ka, amidst enhanced seasonality due to precessional forcing (strongest in SON). This enhanced seasonality leads to greater heat uptake by the lakes and potentially biases the GDGT reconstructions with respect to mean annual air temperature. We demonstrated that the simulated lake energy budget exhibits heightened sensitivity to enhanced MH JJA-SON insolation, with preferential heat uptake in JJA-SON (Sec. 3.2).

Previous studies have demonstrated that GCMs underestimate temperature changes in East African lakes relative to GDGT-based reconstructions [e.g. Loomis et al., 2017]. Our work takes this a step further, evaluating temperature and energy transfers between air and lake surface temperature, as well as potential biases imparted by lake system dynamics. Despite the extended analysis pursued here, we find that while lake system biases can partially account for the model-data discrepancy (up to 0.8°C for some models such as HadGEM2-ES), energy budget biases alone are insufficient to explain the full 1-2.5°C of warming observed during the MH relative to PI in Africa. The multi-model, lake PSM simulation mean provides a quantitative estimate of the offset between lake and air temperatures (+0.3°C) which at best resolves 30% of the observed model-data discrepancy, and at worst, closer to 12% (assuming a maximum warming of 2.5°C). Furthermore, we note that the PMIP3 HIST-PI air temperature mean is approximately 0.3°C for Tanganyika, and 0.2°C for Malawi; thus, the MH warming reconstructed in lake sedimentary archives is not only substantially different from what models show, but also exceeds the range of model HIST-PI differences.

This comparison demands a full account of uncertainties in the model simulations, proxy reconstructions, and the PSM. As mentioned above, GDGT calibration uncertainties vary by reconstruction and method, but can range from 0.4 to 3.7°C [e.g. Tierney et al., 2010a, 2008, Powers et al., 2005, 2010]. Even in a maximum error estimation compounding model ($\pm 0.3°C$, *this study*), proxy ($\pm 0.4°C$,[Tierney et al., 2010a]) and LakePSM parameter uncertainty ($\pm 0.04°C$, *this study*) errors, the model-simulated lake temperatures only graze the lower ($+1°C$) GDGT estimates of relative MH warmth. While there are underconstrained uncertainties in both the models and proxy data, assuming the reconstructions are accurate, it is difficult to imagine that these uncertainties are the primary cause of data-model discrepancy. The GDGT temperature trends, rather than the absolute values, indicate MH warming is robust, and lake system bias can only explain part of the reconstructed temperature change.

As discussed in Section. 3.3, Changes in net downward shortwave radiation, cloud fraction, and temperature anomalies driven by precessional forcing and enhanced seasonality jointly contribute to an amplified lake heating signal. Warmer lake surface temperature in MH SOND compared to HIST is due to: 1) shallowing of mixed layer depths at the end of the dry season occuring earlier in the season (reducing lake heat storage at depth),

2) increased downward shortwave radiation due to orbital forcing accompanied by a decrease in cloudiness during the same months. At Tanganyika, the cumulative effects of decreased evaporation and reduced latent heat loss throughout the dry season at MH compared to HIST could be contributing to warmer SOND temperatures. However, we do not observe a similar decrease in evaporation at Malawi, and Malawi exhibits identical SOND lake surface warming. We conclude that the mixed layer depth and SW effects are the primary drivers of SOND LST warming.

There are important differences between simulated lake climate changes at Tanganyika and Malawi, despite similarities in their seasonal cycle for lake surface temperatures. As noted in Section 3.1 and in Fig. 6, the multi-model average shows [MH-HIST] lake-air offsets of 0.3°C warmer and 0.05°C colder for Tanganyika and Malawi, respectively. In contrast, the GDGT data (Fig. 2b) suggest a similar mid-Holocene warming feature at both Tanganyika and Malawi. This modeled difference between the two lakes can potentially be attributed to differences in shortwave forcing and cloud cover. In HadGEM2-ES, shortwave forcing is elevated in MAM, JJA and SON over Tanganyika, but only in JJA/SON at Malawi (Figs. 7, 8, 9); meanwhile both lakes show reduced or no change in cloud cover for all three seasons (Fig. 10). The total shortwave forcing differs seasonally between the two sites (Figs. 7, 8). This difference might explain the large MH shoaling of the mixed layer in Tanganyika compared to Malawi, though the bias in the LakePSM in simulating Malawi's modern mixed layer depth is large (Table 3). Furthermore, Fig. S4 indicates a large increase (decrease) in evaporation and thus surface cooling (warming) during the MH for Malawi (Tanganyika), which likely contributes to Malawi's simulated colder temperatures. Further diagnostics are required to fully deconvolve this difference.

Nonstationarity in seasonal mixing depths may also generate biases in GDGT temperature reconstructions during the MH. In the present day, the concentrations of GDGT-producing Thaumarchaeota in the water column of Lakes Malawi and Tanganyika are low in the surface mixed layer and increase in the thermocline, below the lakes chlorophyll maxima and in the lakes suboxic zone and oxycline [Schouten et al., 2012, Kumar et al., 2019]. Both theory and our simulations suggest that during the MH, as the lakes warmed, the thermocline shoaled. This is consistent with ongoing changes in Lake Tanganyika, where anthropogenic warming has resulted in a shoaling of the thermocline and oxycline [Cohen et al., 2016]. Kraemer et al. [2015] noted that changes in lake temperature during the last century inferred from TEX_{86} [Tierney et al., 2010a] overestimated observed and modeled temperature changes, and suggested that shoaling of the oxycline, where Thaumarchaeota reside, exposed the GDGT-producers to warmer water within the surface mixed layer. This would increase the amplitude of warming recorded by TEX86. However, shoaling of the thermocline, such as we simulate during the mid-Holocene, could have the opposite effect exposing Thaumarchaeota to colder, deeper waters if the oxycline remains stationary. Furthermore, Hurley et al. [2016] demonstrate that if Thaumarchaeota GDGT producers become ammonium-starved in a particular season, they produce higher TEX_{86}. Thus, the question is how changes in the depth and temperatures within the thermocline, oxycline, chlorophyll maximum, and ultimately the depth of Thaumarachaeotal GDGT production interact during intervals of climate change. While shifts in mixed layer depth are simulated by multiple models, it is at present impossible to conclusively identify the impacts of those changes on the proxy records without an independent proxy for lake surface temperature, mixed layer, and/or oxycline depth. At present, few proxies for mixing depth are available alongside these records. Regardless, simulated changes in mixed layer depth during the MH could cause non-stationary responses of GDGT-inferred temperature to surface warming. Nevertheless, uncertainties generated by non-stationarity in mixing depths will obscure the true heating signal in GDGT reconstructions [Kraemer et al., 2015, Zhu et al., 2017, Zhang and Liu, 2018, Kumar et al., 2019]. Advances developing PSMs of intermediate complexity for TEX_{86} in large, stratified lakes are needed to refine our understanding of these effects.

It is important to contextualize the data-model comparison presented here with temporally coherent paleoclimate archives. Some global syntheses indicate cooling from 6ka-0ka [Marcott et al., 2013, Kaufman et al., 2020b,a], though recent work highlights significant seasonal biases in these reconstructions at higher latitudes [Bova et al., 2021]. Globally, glaciers were advancing during this time in both Greenland and at lower latitudes, such as the Alps [Marcott et al., 2013, Liu et al., 2014, Marsicek et al., 2018]). The observed warming reported in the Tanganyika and Malawi reconstructions is observed in other East African rift lakes, including Turkana [Berke et al., 2012a, Linke et al., 2018, Loomis et al., 2012]. While many of these proxy types respond to multiple climate drivers, we cannot rule out the possibility, based on these multi-proxy lines of evidence, that tropical Africa may have warmed by 1-2°C during the MH, warmer than the historical period. These other proxy data also disagree with the relatively quiescent model simulations (especially transient simulations), which do not indicate abrupt changes in temperature across the MH.

We note additional important caveats of this work. In both Lake Tanganyika and Lake Malawi, oscillation of the thermocline results from southerly winds that generate lake surface water highs at the northern sides of the lakes, which then flow southwards when the winds subside. This creates an oscillation with a period of a few weeks and an amplitude of several tens of meters [e.g. Naithani et al., 2003], and likely impacts mixing depths in these large lakes. The LakePSM used in this paper [Dee et al., 2018] is a one-dimensional model, oversimplying processes in long, deep, narrow lakes such as Malawi and Tanganyika, where thermocline dynamics play an important role in the lake heating budgets. Additional modeling using a three-dimensional coupled lake model would incorporate water column mixing associated with thermocline response to wind fields. This may strongly impact mixing depth and lake surface water temperature. The use of such 3D lake models [e.g. Laval et al., 2003, León et al., 2007] is an important next step forward in the model-data comparison.

Additionally, while GDGT records are not seasonally resolved, they may be seasonally biased; transient simulations show particularly elevated SON temperatures in the MH (SI Fig. S5), exceeding annual mean temperatures by $\sim 1°C$. If GDGT producers are selectively recording lake temperatures in specific months, this may contribute to the data-model discrepancy reported in this work. Research forcing the Lake PSM with seasonal temperatures may shed light on the contributions (or lack-thereof) of potential seasonal biases.

Finally, the PMIP4 mid-Holocene multi-model ensemble experiments were recently published [Kageyama et al., 2020], and initial evaluation performed by Brierley [2020] show that MH air temperatures in Africa are cooler for PMIP4 than for PMIP3. This is due to the fact that PMIP4 employs lower (and more realistic) greenhouse gas concentrations compared to PMIP3. Thus, we expect that the model-data discrepancy we document will increase when PMIP4 results are considered. This work also considers all models in the PMIP3 ensemble regardless of their climatological biases relative to observations. Differences between models' treatment of vegetation and aerosols likely drive large simulation spread, and warrant further investigation [e.g. Liu et al., 2018]. Our future planned analysis of the PMIP4 ensemble will assess the fidelity of the models in reproducing modern climatology in east Africa, in order to generate ensemble means weighted by model skill and in an effort to deduce the model physics that give rise to stronger model-data agreement.

5. Conclusions

We evaluated temperature reconstructions from the African tropics, and compared these data with model simulations to assess the dynamics and drivers of African temperature changes over the Holocene. Studies such as this characterizing past temperature changes and their governing mechanisms are fundamental to understanding future climate change. Further, surface temperature is one of the few climate variables that we can quantitatively reconstruct with reasonable accuracy and precision. Climate models are thought to have greater skill in predicting changes in temperature than hydroclimate variables such as precipitation, yet there are few data-model comparison studies to test this assumption for tropical continental air temperatures. This work analyzes two lake temperature reconstructions from Africa and re-evaluates mean-state temperature transitions resolved in these records using a new PSM. The Lake PSM elucidates relationships between lake and air temperatures (i.e., energy and mass transfers). We show that impacts on the relationship between lake temperature and air temperature can be imparted by lake processes, and these impacts can be quantitatively simulated and partitioned from the primary climate signal. This enhanced data-model comparison provides more realistic constraints on climate model simulations of the past to identify potential shortcomings they face predicting future temperature change in Africa.

Ensemble climate model simulations predict African warming of up to 5°C by 2080-2099 in an RCP8.5 high emissions scenario [IPCC, 2013]; this will severely stress society and ecosystems [Boko, 2007, James and Washington, 2013]. Air temperature affects human health, directly through heat waves causing cardiac and respiratory distress, and indirectly through its impact on disease transmission, drought, agriculture, and ecosystems. Evaluating climate model simulations spanning past warm climates facilitates validation of projections of future warming performed with the same climate models [Taylor et al., 2012], allowing us to systematically evaluate model performance. The temperature reconstructions evaluated here suggest substantial sustained, long-term warming during the MH (Fig. 2b.); while it is possible these warming events in the GDGT record may be an under-constrained artifact of the proxy system, the warming is still notably lacking in current-generation climate models. Careful evaluation of these warming events, such as that of the 6 ka heating event, is crucial for contextualizing patterns and amplitudes of African climate change in the past and future.

In forthcoming research, we hope to amass a greater number of African temperature records for a more complete and heterogeneous view of African temperature evolution. Extension work should synthesize a more geographically comprehensive set of continental temperature reconstructions from Africa and evaluate these reconstructions using lake proxy system models, providing a more robust evaluation of the potential for rapid tropical temperature change. This information is needed to elucidate the drivers of African climate changes, provide better statistics constraining continental African temperature sensitivity, and enable more robust predictions of climate change in Africa for scientists and policy makers.

Acknowledgements

This work was supported by the National Science Foundation (EAR-1903347) awarded to S. Dee, J. Russell, and C. Morrill, and EAR-1903345 awarded to C. Morrill. We thank the editor and Drs. Tom Johnson, Byron Steinman, and Jessica Tierney for their constructive and thorough reviews of this manuscript, which greatly improved this work. We thank Zihan Chen, an undergraduate researcher at Brown University, for completing preliminary calibrations and testing of the lake model. We acknowledge the World Climate Research Programmes Working Group on Coupled Modeling and the Paleoclimate Modelling Intercomparison Project for CMIP/PMIP model output. TraCE-21ka was made possible by the DOE INCITE computing program, and supported by NCAR, the NSF P2C2 program, and the DOE Abrupt Change and EaSM programs. *Data Availability Statement:* CMIP5/PMIP3 simulations are publicly available via `https://esgf-node.llnl.gov/search/cmip5/`. The TraCE-21 ka EXP is publicly available via `earthsystemgrid.org`. LakePSM code is freely available via Zenodo at `https://zenodo.org/record/3890080#.YHW0VEhKhBw`, as well as Github `https://github.com/sylvia-dee/PRYSM/tree/2.0` with DOI: `10.5281/zenodo.3890080`.

R. B. Alley. Ice-core evidence of abrupt climate changes. *Proceedings of the National Academy of Sciences*, 97(4):1331–1334, 2000.

R. B. Alley and P. U. Clark. The deglaciation of the northern hemisphere: a global perspective. *Annual Review of Earth and Planetary Sciences*, 27 (1):149–182, 1999.

P. J. Bartlein and S. L. Shafer. Paleo calendar-effect adjustments in time-slice and transient climate-model simulations (paleocaladjust v1. 0): impact and strategies for data analysis. *Geoscientific Model Development*, 12(9), 2019.

M. A. Berke, T. C. Johnson, J. P. Werne, K. Grice, S. Schouten, and J. S. S. Damsté. Molecular records of climate variability and vegetation response since the late pleistocene in the lake victoria basin, east africa. *Quaternary Science Reviews*, 55:59–74, 2012a.

M. A. Berke, T. C. Johnson, J. P. Werne, S. Schouten, and J. S. S. Damste. A mid-holocene thermal maximum at the end of the african humid period. *Earth and Planetary Science Letters*, 351:95–104, 2012b.

M. Boko. Climate Change 2007: Impacts, Adaptation and Vulnerability. Contribution of Working Group II to the Fourth Assessment Report of the Intergovernmental Panel on Climate Change, 2007.

S. Bova, Y. Rosenthal, Z. Liu, S. P. Godad, and M. Yan. Seasonal origin of the thermal maxima at the holocene and the last interglacial. *Nature*, 589(7843):548–553, 2021.

P. Braconnot, S. P. Harrison, M. Kageyama, P. J. Bartlein, V. Masson-Delmotte, A. Abe-Ouchi, B. Otto-Bliesner, and Y. Zhao. Evaluation of climate models using palaeoclimatic data. *Nature Climate Change*, 2(6): 417–424, 2012.

C. Brierley. Large-scale features and evaluation of the pmip4-cmip6 mid-holocene simulations. *Climate of the Past Discussions*, 2020.

I. S. Castañeda and S. Schouten. A review of molecular organic proxies for examining modern and ancient lacustrine environments. *Quaternary Science Reviews*, 30(21):2851–2891, 2011.

M. Chevalier, S. Brewer, and B. M. Chase. Qualitative assessment of pmip3 rainfall simulations across the eastern african monsoon domains during the mid-holocene and the last glacial maximum. *Quaternary Science Reviews*, 156:107–120, 2017.

P. U. Clark, J. D. Shakun, P. A. Baker, P. J. Bartlein, S. Brewer, E. Brook, A. E. Carlson, H. Cheng, D. S. Kaufman, Z. Liu, et al. Global climate evolution during the last deglaciation. *Proceedings of the National Academy of Sciences*, 109(19):E1134–E1142, 2012.

A. S. Cohen, E. L. Gergurich, B. M. Kraemer, M. M. McGlue, P. B. McIntyre, J. M. Russell, J. D. Simmons, and P. W. Swarzenski. Climate warming reduces fish production and benthic habitat in lake tanganyika, one of the most biodiverse freshwater ecosystems. *Proceedings of the National Academy of Sciences*, 113(34):9563–9568, 2016.

K. Costa, J. Russell, B. Konecky, and H. Lamb. Isotopic reconstruction of the african humid period and congo air boundary migration at lake tana, ethiopia. *Quaternary Science Reviews*, 83:58–67, 2014.

D. P. Dee, S. M. Uppala, A. Simmons, P. Berrisford, P. Poli, S. Kobayashi, U. Andrae, M. Balmaseda, G. Balsamo, d. P. Bauer, et al. The era-interim reanalysis: Configuration and performance of the data assimilation system. *Quarterly Journal of the royal meteorological society*, 137 (656):553–597, 2011.

S. Dee, J. Emile-Geay, M. Evans, A. Allam, E. Steig, and D. Thompson. Prysm: An open-source framework for proxy system modeling, with applications to oxygen-isotope systems. *Journal of Advances in Modeling Earth Systems*, 7(3):1220–1247, 2015.

S. G. Dee, J. M. Russell, C. Morrill, Z. Chen, and A. Neary. Prysm v2. 0: A proxy system model for lacustrine archives. *Paleoceanography and Paleoclimatology*, 33(11):1250–1269, 2018.

A. Detges. Local conditions of drought-related violence in sub-saharan africa: The role of road and water infrastructures. *Journal of peace research*, 53(5):696–710, 2016.

D. H. Eccles. An outline of the physical limnology of lake malawi (lake nyasa). *Limnology and Oceanography*, 19(5):730–742, 1974.

M. Evans, S. Tolwinski-Ward, D. Thompson, and K. Anchukaitis. Applications of proxy system modeling in high resolution paleoclimatology. *Quaternary Science Reviews*, 76(0):16 – 28, 2013. ISSN 0277-3791. doi:

10.1016/j.quascirev.2013.05.024. URL `http://www.sciencedirect.com/science/article/pii/S0277379113002011`.

B. P. Finney and T. C. Johnson. Sedimentation in lake malawi (east africa) during the past 10,000 years: a continuous paleoclimatic record from the southern tropics. *Palaeogeography, Palaeoclimatology, Palaeoecology*, 85 (3-4):351–366, 1991.

P. G Kumambala and A. Ervine. Water balance model of lake malawi and its sensitivity to climate change. *The Open Hydrology Journal*, 4(1), 2010.

F. Gasse. Hydrological changes in the african tropics since the last glacial maximum. *Quaternary Science Reviews*, 19(1):189–211, 2000.

J. Green. Nilotic lakes of the western rift. In *The Nile*, pages 263–286. Springer, 2009.

F. He. *Simulating transient climate evolution of the last deglaciation with CCSM 3*, volume 72. Atmospheric and Oceanic Sciences, University of Wisconsin-Madison, USA, 2011.

S. Hostetler and P. Bartlein. Simulation of lake evaporation with application to modeling lake level variations of harney-malheur lake, oregon. *Water Resources Research*, 26(10):2603–2612, 1990.

S. J. Hurley, F. J. Elling, M. Könneke, C. Buchwald, S. D. Wankel, A. E. Santoro, J. S. Lipp, K.-U. Hinrichs, and A. Pearson. Influence of ammonia oxidation rate on thaumarchaeal lipid composition and the tex86 temperature proxy. *Proceedings of the National Academy of Sciences*, 113 (28):7762–7767, 2016.

IPCC. *Summary for Policymakers*, book section SPM, pages 1–30. Cambridge University Press, Cambridge, United Kingdom and New York, NY, USA, 2013. doi: 10.1017/CBO9781107415324.004. URL `www.climatechange2013.org`.

S. J. Ivory and J. Russell. Climate, herbivory, and fire controls on tropical african forest for the last 60ka. *Quaternary Science Reviews*, 148:101–114, 2016.

R. James and R. Washington. Changes in african temperature and precipitation associated with degrees of global warming. *Climatic change*, 117 (4):859–872, 2013.

T. C. Johnson, E. T. Brown, J. McManus, S. Barry, P. Barker, and F. Gasse. A high-resolution paleoclimate record spanning the past 25,000 years in southern east africa. *Science*, 296(5565):113–132, 2002.

F. Joos and R. Spahni. Rates of change in natural and anthropogenic radiative forcing over the past 20,000 years. *Proceedings of the National Academy of Sciences*, 105(5):1425–1430, 2008.

M. Kageyama, S. P. Harrison, M.-L. Kapsch, M. Löfverström, J. M. Lora, U. Mikolajewicz, S. Sherriff-Tadano, T. Vadsaria, A. Abe-Ouchi, N. Bouttes, et al. The pmip4-cmip6 last glacial maximum experiments: preliminary results and comparison with the pmip3-cmip5 simulations. *Climate of the Past*, 2020.

D. Kaufman, N. McKay, C. Routson, M. Erb, C. Dätwyler, P. S. Sommer, O. Heiri, and B. Davis. Holocene global mean surface temperature, a multi-method reconstruction approach. *Scientific data*, 7(1):1–13, 2020a.

D. Kaufman, N. McKay, C. Routson, M. Erb, B. Davis, O. Heiri, S. Jaccard, J. Tierney, C. Dätwyler, Y. Axford, et al. A global database of holocene paleotemperature records. *Scientific data*, 7(1):1–34, 2020b.

B. M. Kraemer, S. Hook, T. Huttula, P. Kotilainen, C. M. O'Reilly, A. Peltonen, P.-D. Plisnier, J. Sarvala, R. Tamatamah, Y. Vadeboncoeur, et al. Century-long warming trends in the upper water column of lake tanganyika. *PLoS One*, 10(7):e0132490, 2015.

D. M. Kumar, M. Woltering, E. C. Hopmans, J. S. S. Damsté, S. Schouten, and J. P. Werne. The vertical distribution of thaumarchaeota in the water column of lake malawi inferred from core and intact polar tetraether lipids. *Organic geochemistry*, 132:37–49, 2019.

B. Laval, J. Imberger, B. R. Hodges, and R. Stocker. Modeling circulation in lakes: Spatial and temporal variations. *Limnology and Oceanography*, 48(3):983–994, 2003.

L. F. León, D. C.-L. Lam, W. Schertzer, D. A. Swayne, and J. Imberger. Towards coupling a 3d hydrodynamic lake model with the canadian regional climate model: simulation on great slave lake. *Environmental Modelling & Software*, 22(6):787–796, 2007.

A. M. Linke, F. D. Witmer, J. OLoughlin, J. T. McCabe, and J. Tir. Drought, local institutional contexts, and support for violence in kenya. *Journal of Conflict Resolution*, 62(7):1544–1578, 2018.

Y. Liu, M. Zhang, Z. Liu, Y. Xia, Y. Huang, Y. Peng, and J. Zhu. A possible role of dust in resolving the holocene temperature conundrum. *Scientific reports*, 8(1):1–9, 2018.

Z. Liu, B. Otto-Bliesner, F. He, E. Brady, R. Tomas, P. Clark, A. Carlson, J. Lynch-Stieglitz, W. Curry, E. Brook, et al. Transient simulation of last deglaciation with a new mechanism for bølling-allerød warming. *Science*, 325(5938):310–314, 2009.

Z. Liu, J. Zhu, Y. Rosenthal, X. Zhang, B. L. Otto-Bliesner, A. Timmermann, R. S. Smith, G. Lohmann, W. Zheng, and O. E. Timm. The holocene temperature conundrum. *Proceedings of the National Academy of Sciences*, 111(34):E3501–E3505, 2014.

S. E. Loomis, J. M. Russell, B. Ladd, F. A. Street-Perrott, and J. S. S. Damsté. Calibration and application of the branched gdgt temperature proxy on east african lake sediments. *Earth and Planetary Science Letters*, 357:277–288, 2012.

S. E. Loomis, J. M. Russell, D. Verschuren, C. Morrill, G. De Cort, J. S. S. Damsté, D. Olago, H. Eggermont, F. A. Street-Perrott, and M. A. Kelly. The tropical lapse rate steepened during the last glacial maximum. *Science advances*, 3(1):e1600815, 2017.

D. J. Lorenz, D. Nieto-Lugilde, J. L. Blois, M. C. Fitzpatrick, and J. W. Williams. Downscaled and debiased climate simulations for north america from 21,000 years ago to 2100ad. *Scientific data*, 3(1):1–19, 2016.

S. A. Marcott, J. D. Shakun, P. U. Clark, and A. C. Mix. A reconstruction of regional and global temperature for the past 11,300 years. *science*, 339 (6124):1198–1201, 2013.

J. Marsicek, B. N. Shuman, P. J. Bartlein, S. L. Shafer, and S. Brewer. Reconciling divergent trends and millennial variations in holocene temperatures. *Nature*, 554(7690):92, 2018.

M. Meinshausen, S. Smith, K. Calvin, J. Daniel, M. Kainuma, J. Lamarque, K. Matsumoto, S. Montzka, S. Raper, K. Riahi, et al. The paleoclimate modeling intercomparison project contribution to cmip5. *WCRP Coupled Model Intercomparison Project-Phase 5-CMIP5*, page 15, 2011.

A. S. Minale. Water level fluctuations of lake tana and its implication on local communities livelihood, northwestern ethiopia. *International Journal of River Basin Management*, 18(4):503–510, 2020.

A. Morrissey, C. A. Scholz, and J. M. Russell. Late quaternary tex86 paleotemperatures from the world's largest desert lake, lake turkana, kenya. *Journal of Paleolimnology*, pages 1–15, 2017.

J. Naithani, E. Deleersnijder, and P.-D. Plisnier. Analysis of wind-induced thermocline oscillations of lake tanganyika. *Environmental Fluid Mechanics*, 3(1):23–39, 2003.

L. Powers, J. P. Werne, A. J. Vanderwoude, J. S. S. Damsté, E. C. Hopmans, and S. Schouten. Applicability and calibration of the tex86 paleothermometer in lakes. *Organic Geochemistry*, 41(4):404–413, 2010.

L. A. Powers, T. C. Johnson, J. P. Werne, I. S. Castaneda, E. C. Hopmans, J. S. Sinninghe Damsté, and S. Schouten. Large temperature variability in the southern african tropics since the last glacial maximum. *Geophysical Research Letters*, 32(8), 2005.

W. F. Ruddiman. Orbital insolation, ice volume, and greenhouse gases. *Quaternary Science Reviews*, 22(15-17):1597–1629, 2003.

J. M. Russell, H. Vogel, B. L. Konecky, S. Bijaksana, Y. Huang, M. Melles, N. Wattrus, K. Costa, and J. W. King. Glacial forcing of central indonesian hydroclimate since 60,000 y bp. *Proceedings of the National Academy of Sciences*, 111(14):5100–5105, 2014.

J. M. Russell, E. C. Hopmans, S. E. Loomis, J. Liang, and J. S. S. Damsté. Distributions of 5-and 6-methyl branched glycerol dialkyl glycerol tetraethers (brgdgts) in east african lake sediment: Effects of temperature, ph, and new lacustrine paleotemperature calibrations. *Organic Geochemistry*, 117:56–69, 2018.

S. Schouten, E. C. Hopmans, E. Schefuß, and J. S. S. Damste. Distributional variations in marine crenarchaeotal membrane lipids: a new tool for reconstructing ancient sea water temperatures? *Earth and Planetary Science Letters*, 204(1-2):265–274, 2002.

S. Schouten, W. I. C. Rijpstra, E. Durisch-Kaiser, C. J. Schubert, and J. S. S. Damsté. Distribution of glycerol dialkyl glycerol tetraether lipids in the water column of lake tanganyika. *Organic geochemistry*, 53:34–37, 2012.

J. D. Shakun and A. E. Carlson. A global perspective on last glacial maximum to holocene climate change. *Quaternary Science Reviews*, 29(15-16): 1801–1816, 2010.

T. M. Shanahan, N. P. McKay, K. A. Hughen, J. T. Overpeck, B. Otto-Bliesner, C. W. Heil, J. King, C. A. Scholz, and J. Peck. The time-transgressive termination of the african humid period. *Nature Geoscience*, 8(2):140, 2015.

R. Spigel and G. Coulter. Comparison of hydrology and physical limnology of the east african great lakes: Tanganyika, malawi, victoria, kivu and turkana (with reference to some north american great lakes). In *Limnology, climatology and paleoclimatology of the East African lakes*, pages 103–139. Routledge, 2019.

K. E. Taylor, R. J. Stouffer, and G. A. Meehl. An overview of cmip5 and the experiment design. *Bulletin of the American Meteorological Society*, 93(4):485–498, 2012.

J. E. Tierney, J. M. Russell, Y. Huang, J. S. S. Damsté, E. C. Hopmans, and A. S. Cohen. Northern hemisphere controls on tropical southeast african climate during the past 60,000 years. *Science*, 322(5899):252–255, 2008.

J. E. Tierney, M. T. Mayes, N. Meyer, C. Johnson, P. W. Swarzenski, A. S. Cohen, and J. M. Russell. Late-twentieth-century warming in lake tanganyika unprecedented since ad 500. *Nature Geoscience*, 3(6):422–425, 2010a.

J. E. Tierney, D. W. Oppo, Y. Rosenthal, J. M. Russell, and B. K. Linsley. Coordinated hydrological regimes in the indo-pacific region during the past two millennia. *Paleoceanography*, 25(1), 2010b.

J. E. Tierney, J. M. Russell, and Y. Huang. A molecular perspective on late quaternary climate and vegetation change in the lake tanganyika basin, east africa. *Quaternary Science Reviews*, 29(5):787–800, 2010c.

J. E. Tierney, S. C. Lewis, B. I. Cook, A. N. LeGrande, and G. A. Schmidt. Model, proxy and isotopic perspectives on the East African Humid Period. *Earth and Planetary Science Letters*, 307(1):103–112, 2011. doi: 10.1016/j.epsl.2011.04.038.

J. E. Tierney, C. C. Ummenhofer, and P. B. deMenocal. Past and future rainfall in the horn of africa. *Science advances*, 1(9):e1500682, 2015.

B. F. Turner, L. Gardner, and W. Sharp. The hydrology of lake bosumtwi, a climate-sensitive lake in ghana, west africa. *Journal of hydrology*, 183 (3-4):243–261, 1996.

N. von Uexkull. Sustained drought, vulnerability and civil conflict in sub-saharan africa. *Political Geography*, 43:16–26, 2014.

C. Waelbroeck, A. Paul, M. Kucera, A. Rosell-Melé, M. Weinelt, R. Schneider, A. Mix, A. Abelmann, L. Armand, and P. M. MARGO. Constraints on the magnitude and patterns of ocean cooling at the last glacial maximum. *Nature Geoscience*, 2(2):127, 2009.

J. W. Weijers, S. Schouten, J. C. van den Donker, E. C. Hopmans, and J. S. S. Damsté. Environmental controls on bacterial tetraether membrane lipid distribution in soils. *Geochimica et Cosmochimica Acta*, 71(3):703–713, 2007.

M. Wooster, G. Patterson, R. Loftie, and C. Sear. Derivation and validation of the seasonal thermal structure of lake malawi using multi-satellite avhrr observations. *International Journal of Remote Sensing*, 22(15):2953–2972, 2001.

Y. G. Zhang and X. Liu. Export depth of the tex86 signal. *Paleoceanography and Paleoclimatology*, 33(7):666–671, 2018.

J. Zhu, Z. Liu, E. Brady, B. Otto-Bliesner, J. Zhang, D. Noone, R. Tomas, J. Nusbaumer, T. Wong, A. Jahn, et al. Reduced enso variability at the lgm revealed by an isotope-enabled earth system model. *Geophysical Research Letters*, 44(13):6984–6992, 2017.

Figure 1: **Climate forcing from the LGM to present, and African Temperature Evolution**. (A) Radiative forcing from atmospheric CO_2, CH_4, and N_2O (blue), as calculated by Joos and Spahni [2008]; and mean annual (solid orange) and MH calendar-corrected September-October-November (SON, red dashed) insolation at the equator, both in units of W/m^2.

Figure 2: Individual GDGT reconstructions evaluated in this work, comparison with Climate Model Simulations. Simulated vs. reconstructed tropical African temperature, plotted as anomalies relative to PI. GDGT-based temperature reconstructions from Lake Tanganyika (purple) and Lake Malawi (black/grey), with bootstrapped calibration uncertainty ($\sigma = \pm 0.4°C$) as computed in Tierney et al. [2010a]). (A) LGM to PI, reconstructions only. (B) Holocene temperature reconstructions with comparison to model simulations. The brGDGT-based lake temperature reconstructions exhibit a larger amplitude of temperature change (lake temperature) than do transient (CCSM3) and time-slice (PMIP3) GCM simulations of air temperature. All model time series and time slice data are displayed as anomalies relative to pre-industrial values (PI-1850 C.E.) due to the temporal extent of the proxy reconstructions (they do not extend into the modern period). Box plots (grey/black) show the inter-quartile [.25:.75] range (IQR) for the 13 PMIP3 simulations; outlier temperatures are shown in red. PMIP3 model uncertainties are approximately $\pm 0.3°C$, computed by calculating the standard deviation of the [MH-PI] or [MH-HIST] differences for the model ensemble (in terms of annual average air temperature) (and see Table 4). Model data are equilibrium simulations with 1850 C.E. prescribed climate forcing (see citations, Table 2). Note the choice to compute anomalies relative to the PI is due to the fact that lake reconstructions (GDGT records) do not extend into the PMIP3 simulations historical period. The reconstructions are coarse temporally compared to the model simulations. The two PI time periods for the reconstructions were taken as the average of 1750 B.P. (200 C.E.) to 250 B.P. (1700 C.E.) for Malawi (n = 3) and 2818 B.P. (-868 CE) to 1313 B.P. (637 C.E.) for Tanganyika (n = 6).

Figure 3: **Schematic of Lake Heat Budget Terms.** The figure details all the terms which alter the lake temperature profile in the Lake PSM. A full schematic showing all PSM variables (input/output) is available in [Dee et al., 2018]. Approximate heat fluxes are given for each term in W/m^2 (and see Figs. 7, 8).

Figure 4: HadGEM2-Mid Holocene Seasonal Temperature Anomalies (MH minus HIST, calendar-corrected), degrees Celsius [$°C$]. Top left: DJF. Top right: MAM. Bottom left: JJA. Bottom right: SON.

Figure 5: Annual Average Air Temperatures and modeled lake surface temperatures. HadGEM2-ES Mid Holocene vs. Historical Lake Model Simulation Results. (A) 2m Air Temperature (°C) from the HadGEM2-ES PMIP3 simulations for MH and HIST, as well as the ERA-Interim Reanalysis 2m air temperatures for Tanganyika (1979-2017). (B) Simulated lake surface temperature for MH (red) and modern period (ERA-Interim Reanalysis) (blue). (C) Mid Holocene Shortwave Radiation for MH and modern at Lake Tanganyika, highlighting differences in seasonal shortwave radiation reaching surface during MH. (D) Mixing Depth Changes for the modern and MH. In all panels, the MH is plotted in red, and modern period is plotted in blue.

Figure 6: Lake temperature anomaly minus air temperature anomaly [LAKE-AIR] for all PMIP3 Models at (A) Lake Tanganyika and (B) Lake Malawi, MH minus modern (ERA-Interim). The MH lake temperature anomalies are, on average, 0.32°C hotter and 0.05°C colder at Tanganyika and Malawi, respectively, than air temp anomalies. Note that BCC anomalies are likely very low due to greatly increased wind speeds compared to other models during the MH, which amplifies lake cooling.

Figure 7: HadGEM2-ES: MH (colors, dashed) vs. HIST (black) Lake Heat Budget Terms for the Lake Tanganyika simulation. All MH variables are calendar-corrected. A. Lake Surface Temperature (C), B. Mixed Layer Depth (m), C. Latent Heat flux at lake surface (W/m^2), proxy for evaporation, D. Sensible heat flux at lake surface (W/m^2), E. incident shortwave radiation (W/m^2), F. longwave radiation (upwards from lake surface, W/m^2), G. wind speed (m/s), H. downwelling longwave radiation (W/m^2).

Figure 8: HadGEM2-ES: MH (colors, dashed) vs. HIST (black) Lake Heat Budget Terms for the Lake Malawi simulation. All MH variables are calendar-corrected. A. Lake Surface Temperature (C), B. Mixed Layer Depth (m), C. Latent Heat flux at lake surface (W/m^2), proxy for evaporation, D. Sensible heat flux at lake surface (W/m^2), E. incident shortwave radiation (W/m^2), F. longwave radiation (upwards from lake surface, W/m^2), G. wind speed (m/s), H. downwelling longwave radiation (W/m^2).

Figure 9: HadGEM2-ES: MH-HIST Surface Downwelling Shortwave Radiation Anomalies [CLEARSKY], in units of Watts per meter squared [W/m^2]; all MH variables are calendar-corrected. (a) DJF, (b) MAM, (c) JJA, (d) SON.

Figure 10: HadGEM2 (MH-HIST) Cloud Area Fraction (%) (A, B, E, F) Anomalies and Seasonal Precipitation (B, D, G, D) Anomalies over Africa [mm/day]. All MH variables are calendar-corrected. (A, C) DJF, (B, D) MAM, (E, G) JJA, (F, H) SON.

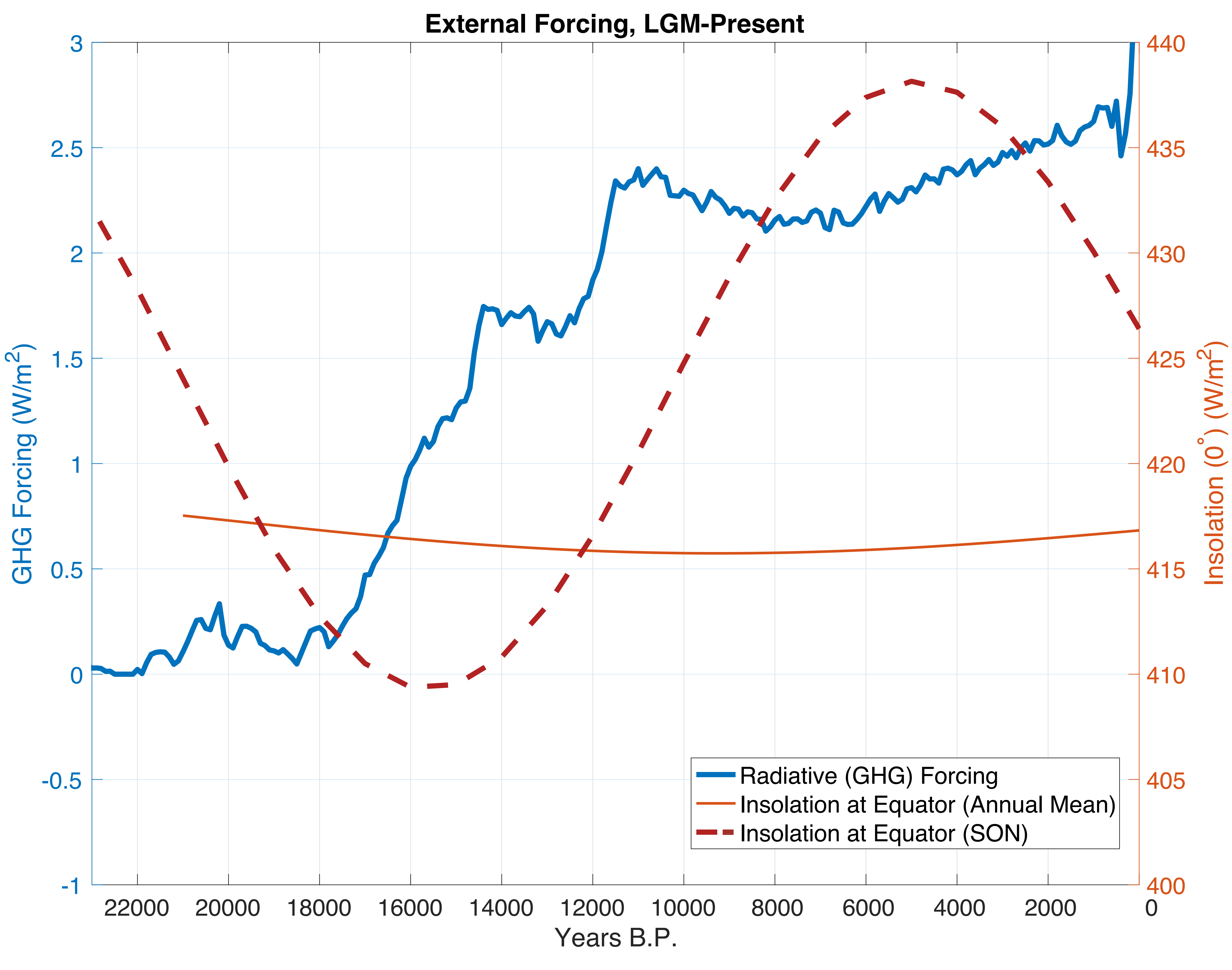
External Forcing, LGM-Present
GHG Forcing (W/m^2)
Insolation (0°) (W/m^2)
Years B.P.
3
2.5
2
1.5
1
0.5
0
-0.5
-1
440
435
430
425
420
415
410
405
400
22000
20000
18000
16000
14000
12000
10000
8000
6000
4000
2000
0
Radiative (GHG) Forcing
Insolation at Equator (Annual Mean)
Insolation at Equator (SON)

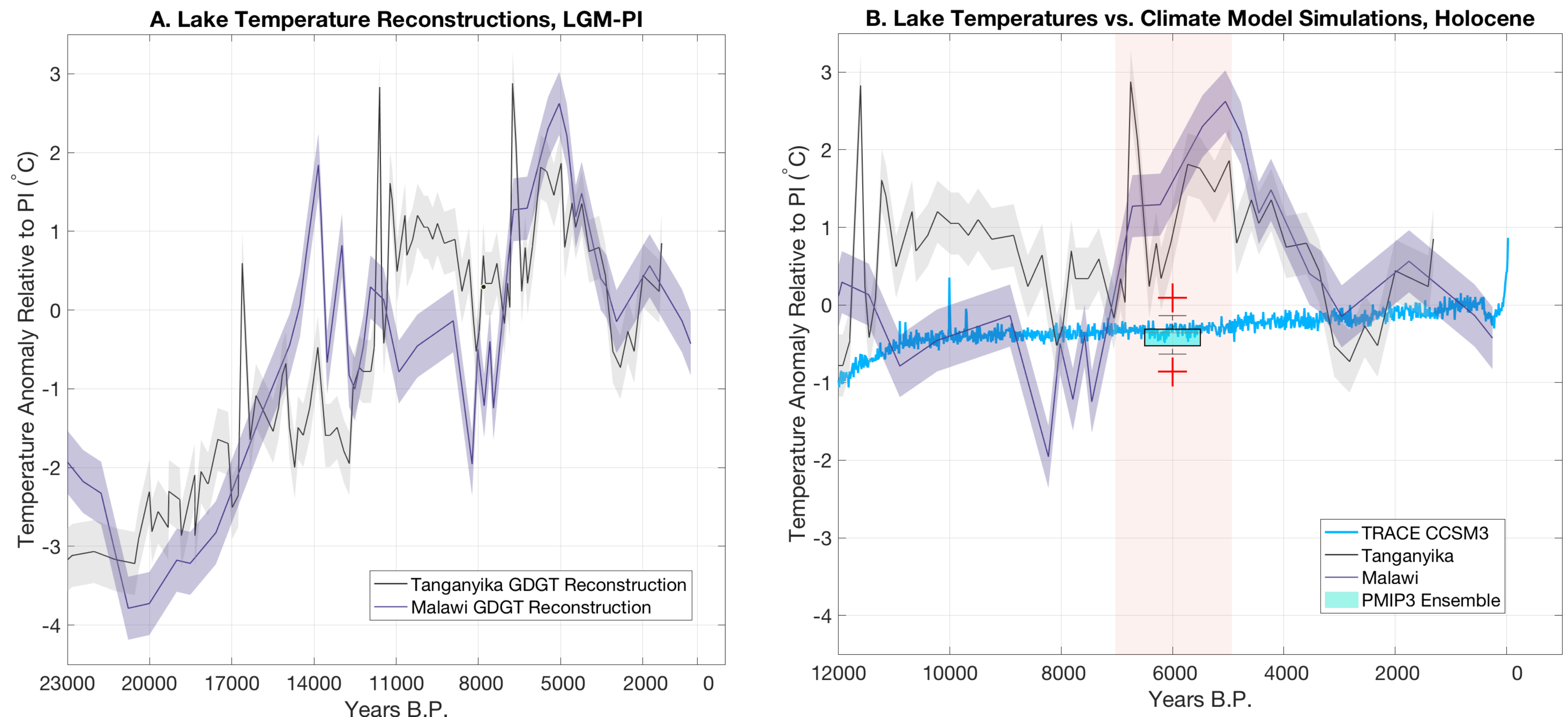
A. Lake Temperature Reconstructions, LGM-PI
Temperature Anomaly Relative to PI (°C)
3
2
1
0
-1
-2
-3
-4
23000
20000
17000
14000
11000
8000
5000
2000
0
Years B.P.
Tanganyika GDGT Reconstruction
Malawi GDGT Reconstruction
B. Lake Temperatures vs. Climate Model Simulations, Holocene
Temperature Anomaly Relative to PI (°C)
3
2
1
0
-1
-2
-3
-4
12000
10000
8000
6000
4000
2000
0
Years B.P.
TRACE CCSM3
Tanganyika
Malawi
PMIP3 Ensemble

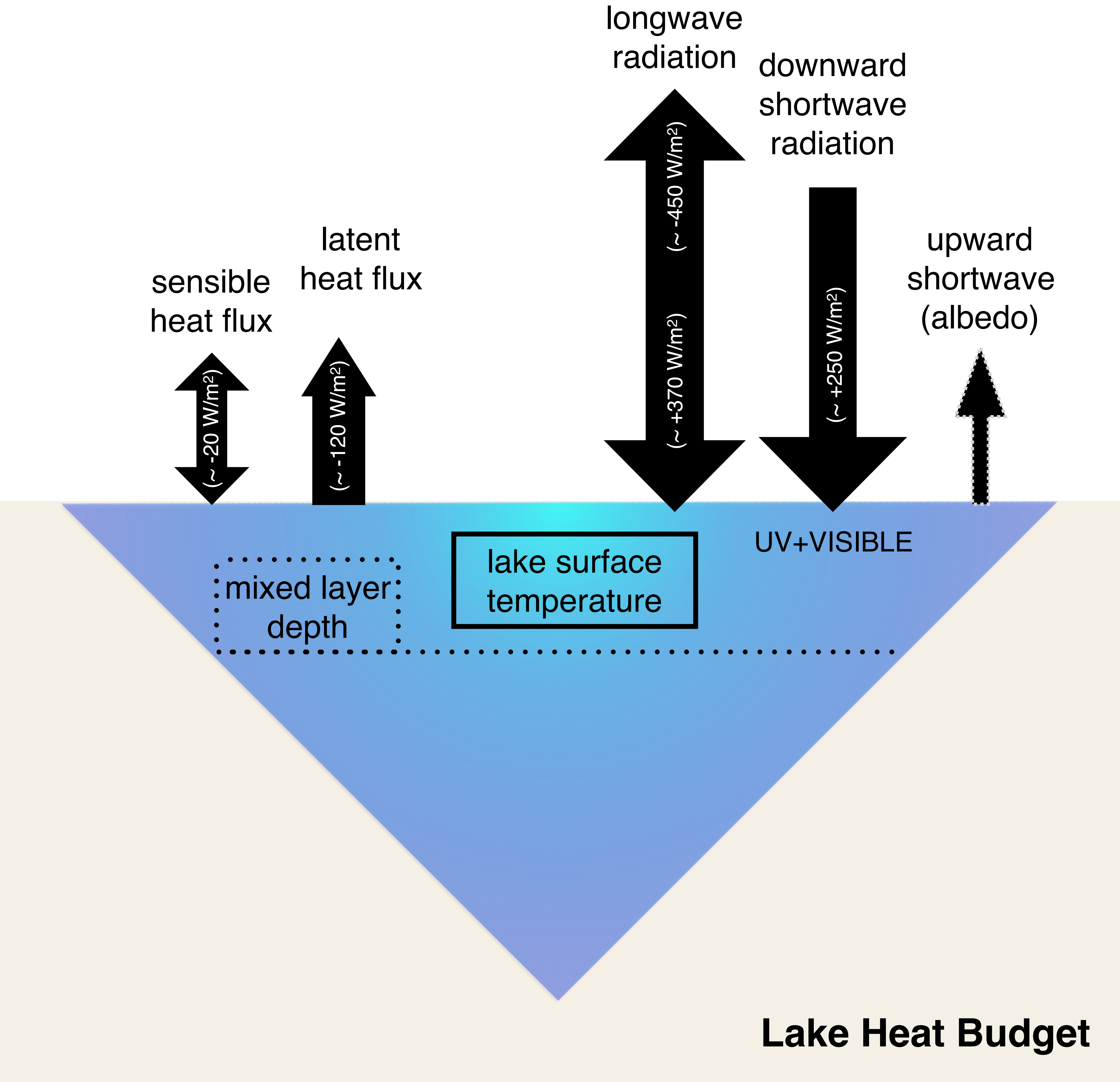
longwave radiation
downward shortwave radiation
(~ -450 W/m²)
(~ +370 W/m²)
(~ +250 W/m²)
latent heat flux
sensible heat flux
upward shortwave (albedo)
(~ -20 W/m²)
(~ -120 W/m²)
UV+VISIBLE
lake surface temperature
mixed layer depth
Lake Heat Budget

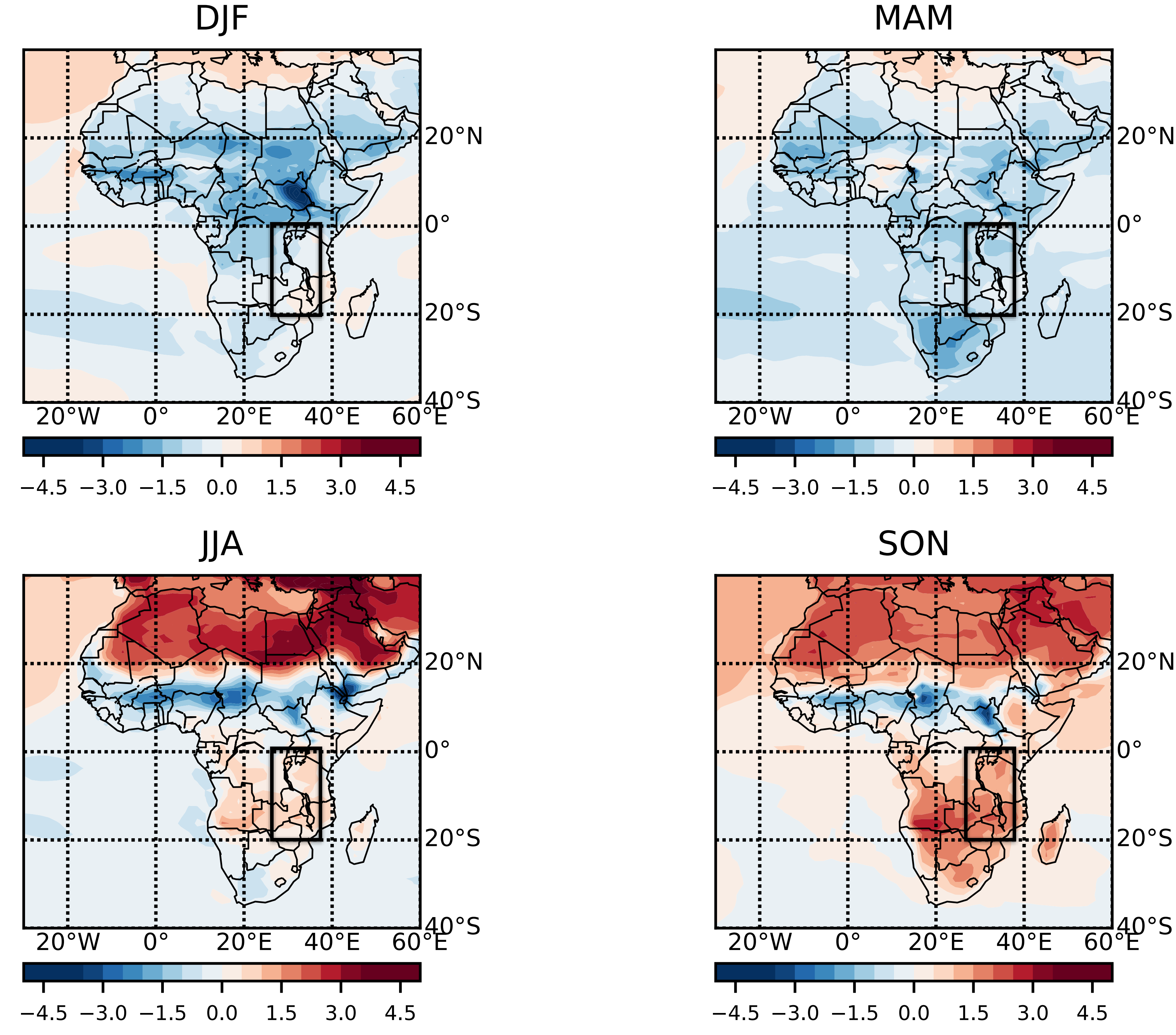

DJF
MAM
JJA
SON
20°N
0°
20°S
40°S
20°W
0°
20°E
40°E
60°E
−4.5
−3.0
−1.5
0.0
1.5
3.0
4.5

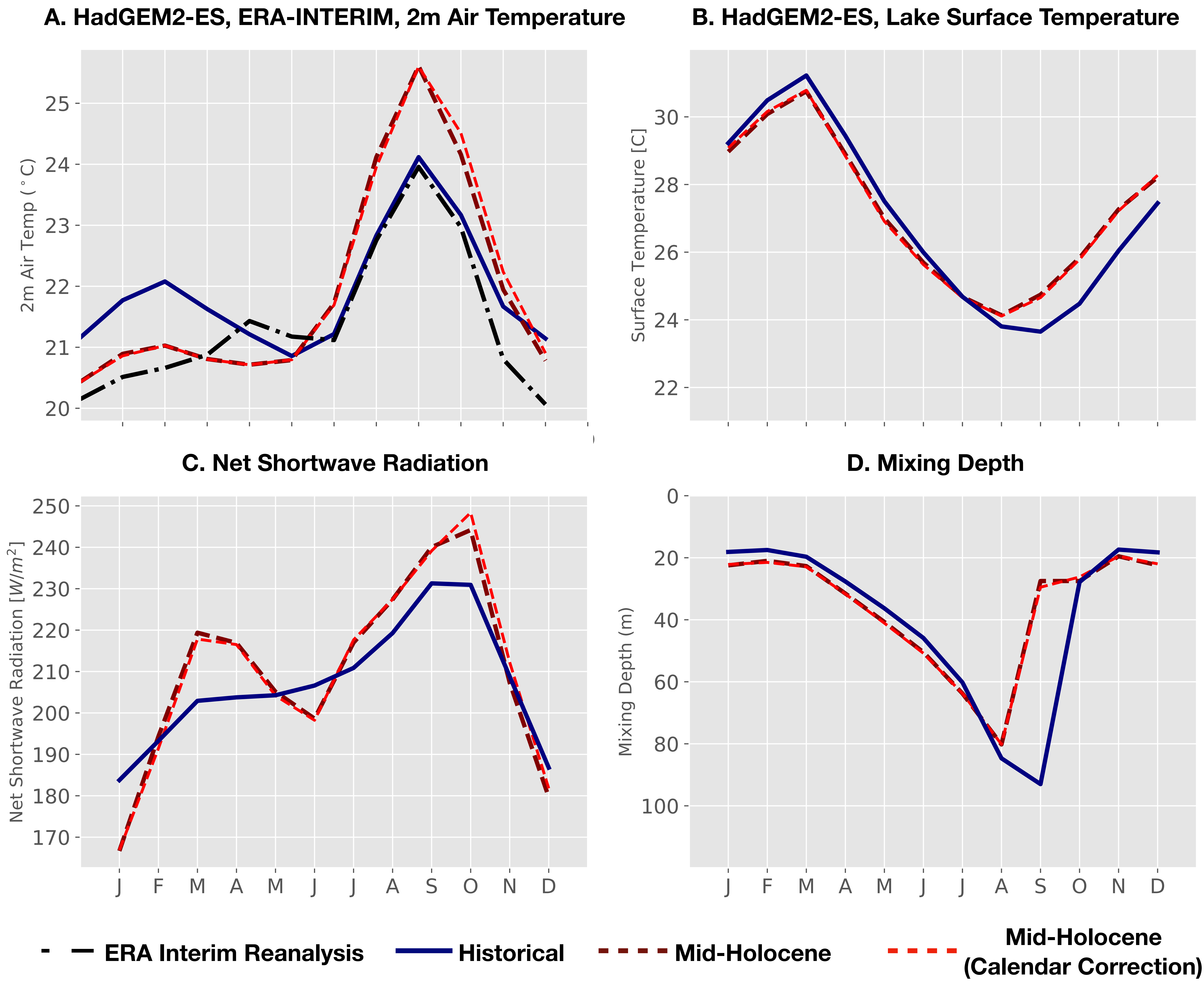
A. HadGEM2-ES, ERA-INTERIM, 2m Air Temperature
B. HadGEM2-ES, Lake Surface Temperature
C. Net Shortwave Radiation
D. Mixing Depth
2m Air Temp (°C)
Surface Temperature [C]
Net Shortwave Radiation [W/m²]
Mixing Depth (m)
J F M A M J J A S O N D
ERA Interim Reanalysis
Historical
Mid-Holocene
Mid-Holocene (Calendar Correction)

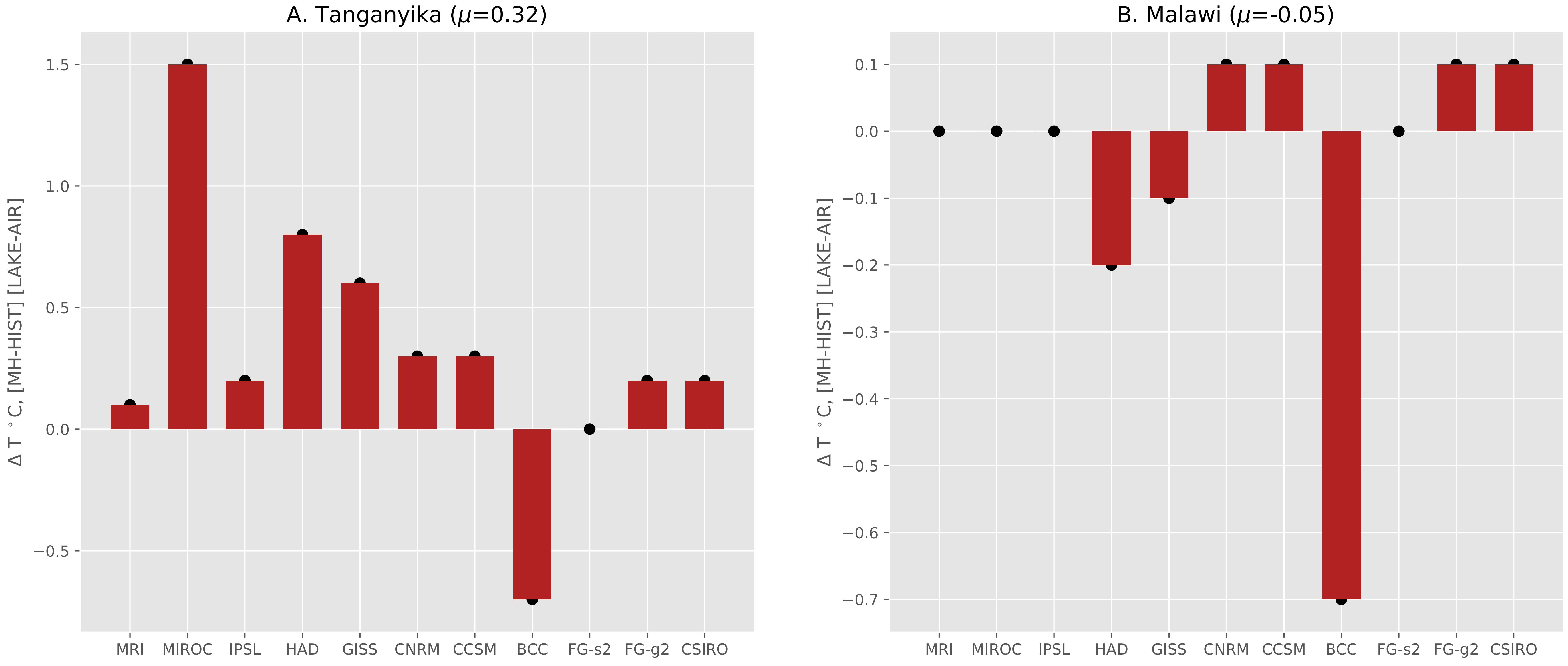

A. Tanganyika (μ=0.32)
B. Malawi (μ=-0.05)
Δ T °C, [MH-HIST] [LAKE-AIR]
1.5
1.0
0.5
0.0
−0.5
0.1
0.0
−0.1
−0.2
−0.3
−0.4
−0.5
−0.6
−0.7
MRI
MIROC
IPSL
HAD
GISS
CNRM
CCSM
BCC
FG-s2
FG-g2
CSIRO

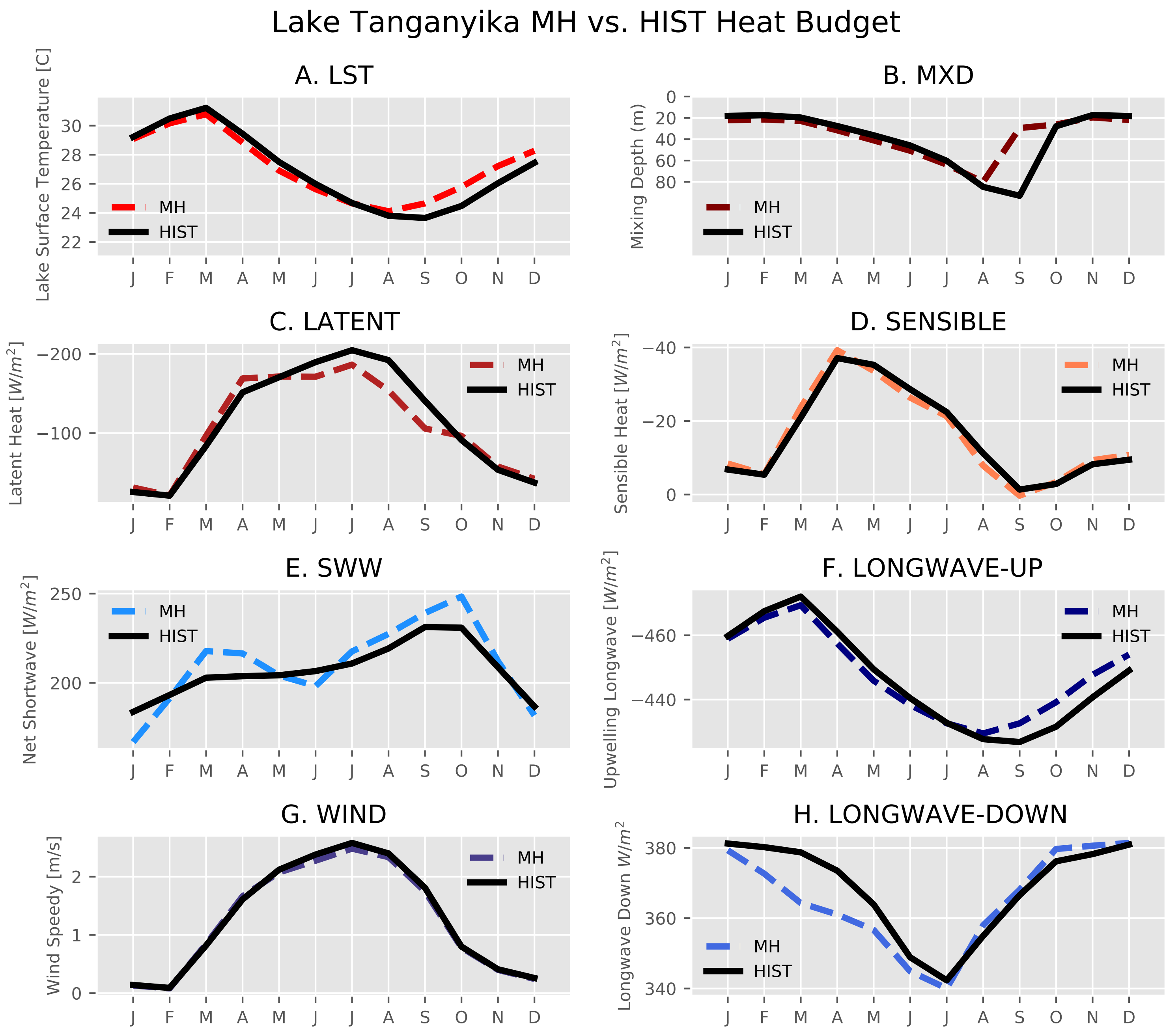

Lake Tanganyika MH vs. HIST Heat Budget
A. LST
Lake Surface Temperature [C]
B. MXD
Mixing Depth (m)
C. LATENT
Latent Heat [W/m^2]
D. SENSIBLE
Sensible Heat [W/m^2]
E. SWW
Net Shortwave [W/m^2]
F. LONGWAVE-UP
Upwelling Longwave [W/m^2]
G. WIND
Wind Speedy [m/s]
H. LONGWAVE-DOWN
Longwave Down W/m^2
MH
HIST
J F M A M J J A S O N D

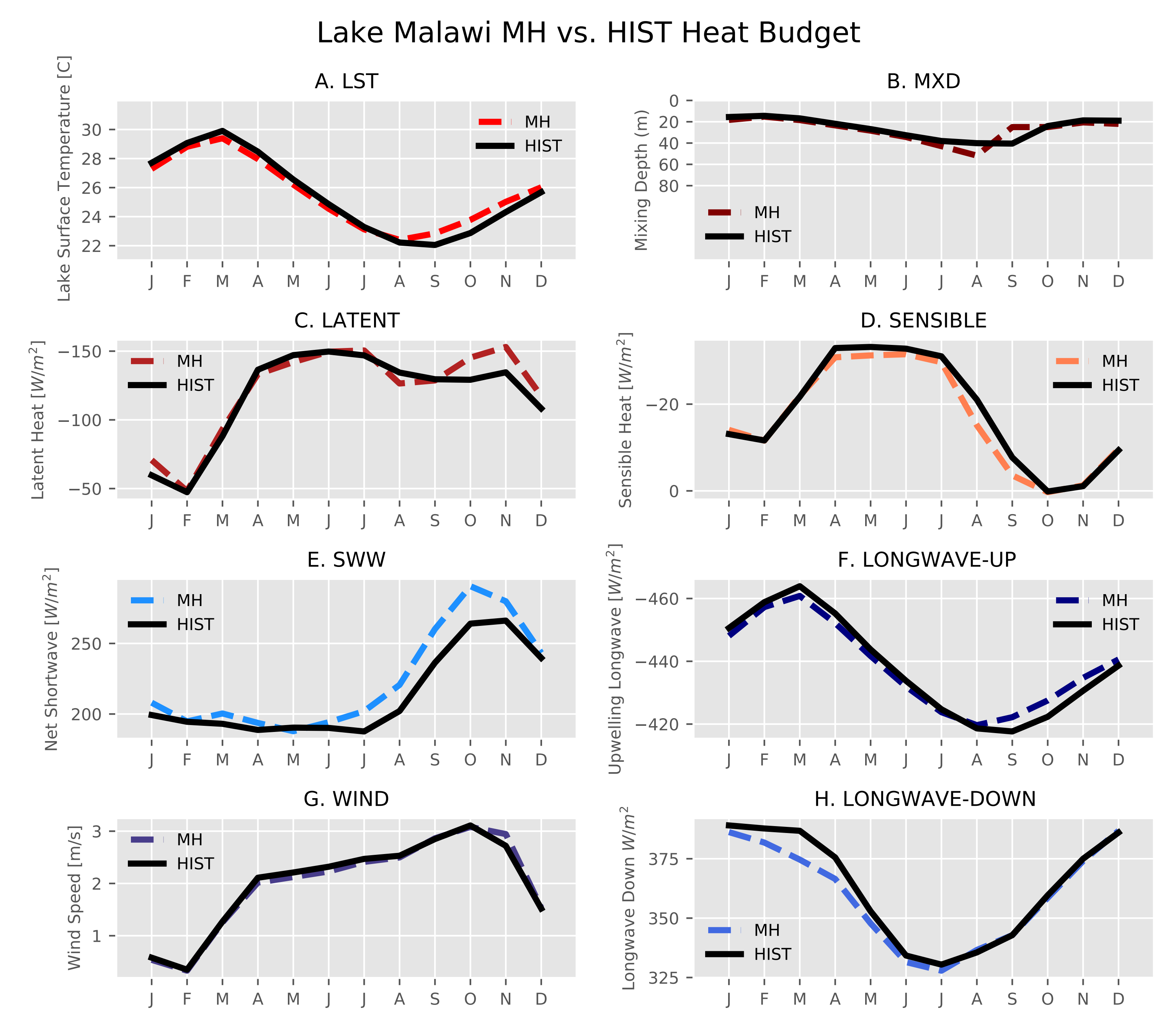

Lake Malawi MH vs. HIST Heat Budget
A. LST
Lake Surface Temperature [C]
MH
HIST
B. MXD
Mixing Depth (m)
C. LATENT
Latent Heat [W/m^2]
D. SENSIBLE
Sensible Heat [W/m^2]
E. SWW
Net Shortwave [W/m^2]
F. LONGWAVE-UP
Upwelling Longwave [W/m^2]
G. WIND
Wind Speed [m/s]
H. LONGWAVE-DOWN
Longwave Down W/m^2
J F M A M J J A S O N D

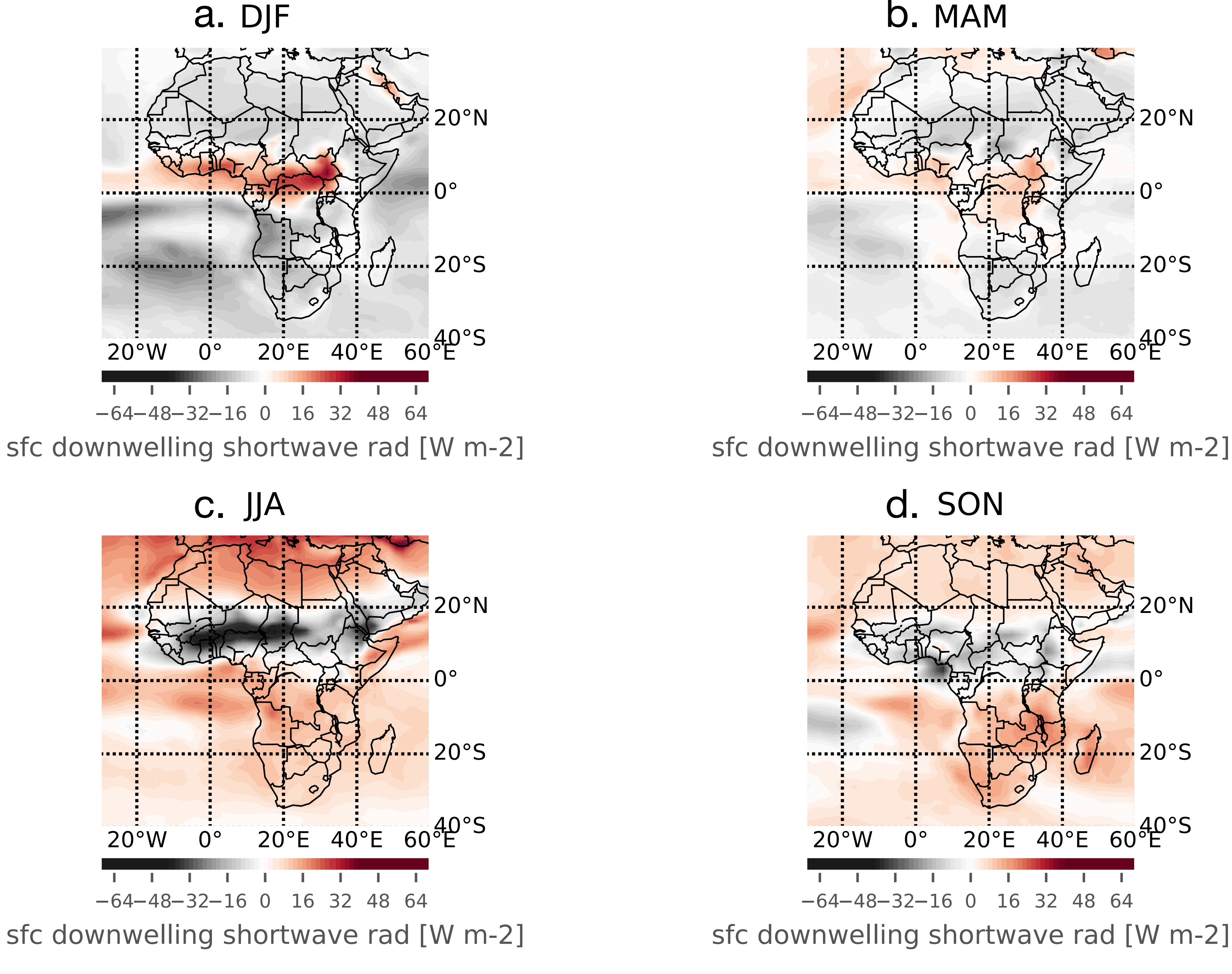
a. DJF
b. MAM
c. JJA
d. SON
20°N
0°
20°S
40°S
20°W
0°
20°E
40°E
60°E
−64
−48
−32
−16
0
16
32
48
64
sfc downwelling shortwave rad [W m-2]

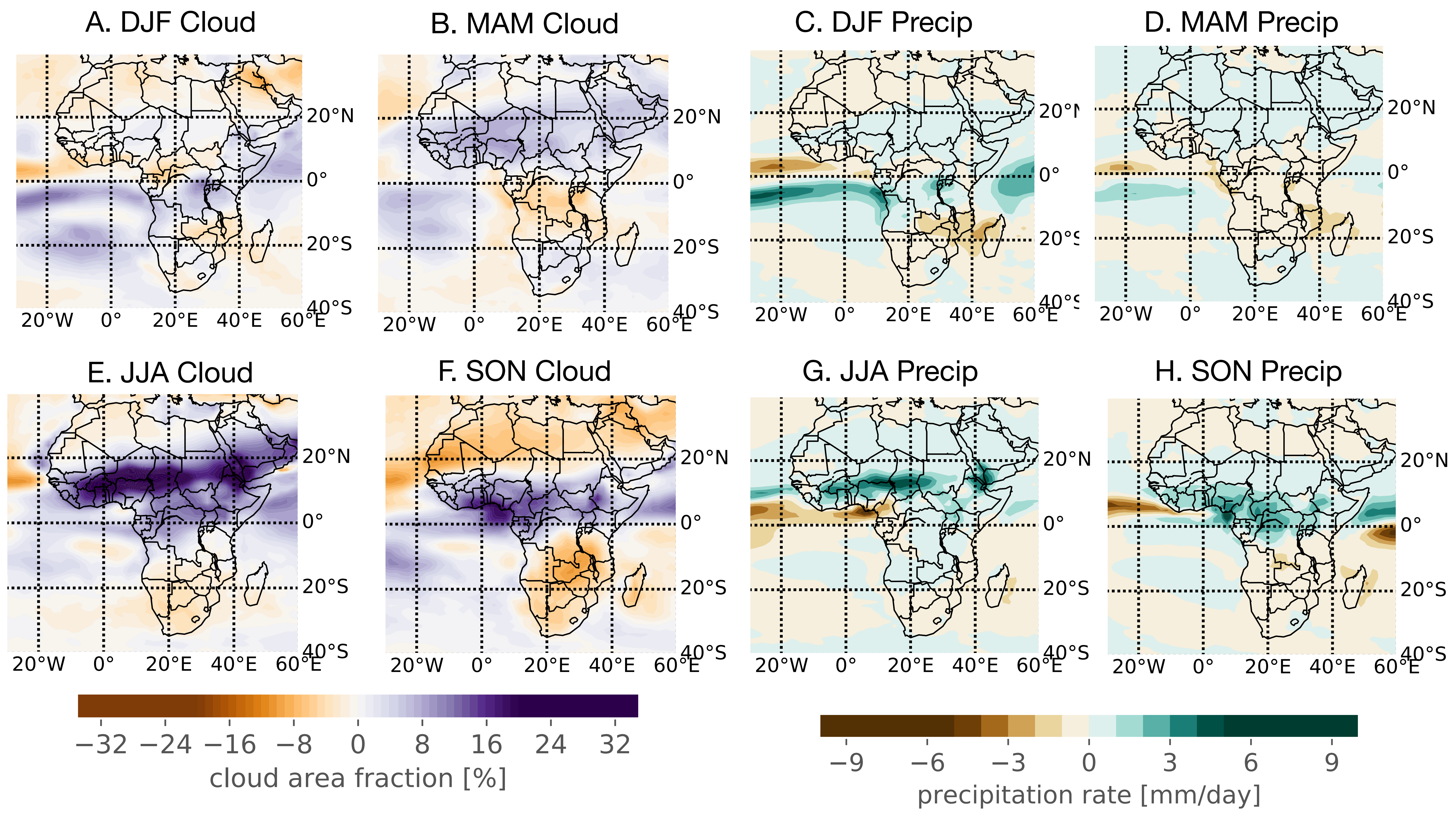

A. DJF Cloud
B. MAM Cloud
C. DJF Precip
D. MAM Precip
E. JJA Cloud
F. SON Cloud
G. JJA Precip
H. SON Precip
20°N
0°
20°S
40°S
20°W
0°
20°E
40°E
60°E
−32
−24
−16
−8
0
8
16
24
32
cloud area fraction [%]
−9
−6
−3
0
3
6
9
precipitation rate [mm/day]